11-1986

Mesoscale Hydrographic Variability in the Vicinity of Points Conception and Arguello During April May 1983: The OPUS 1983 Experiment

Larry P. Atkinson
Old Dominion University, latkinso@odu.edu

Kenneth H. Brink

Russ E. Davis

Burton H. Jones

Theresa Paluszkiewicz

See next page for additional authors

Original Publication Citation

Atkinson, L.P., Brink, K.H., Davis, R.E., Jones, B.H., Paluszkiewicz, T., & Stuart, D.W. (1986). Mesoscale hydrographic variability in the vicinity of Points Conception and Arguello during April May 1983: The OPUS 1983 experiment. *Journal of Geophysical Research: Oceans, 91*(C11), 2899-12918. doi: 10.1029/JC091iC11p12899

Authors
Larry P. Atkinson, Kenneth H. Brink, Russ E. Davis, Burton H. Jones, Theresa Paluszkiewicz, and David W. Stuart

JOURNAL OF GEOPHYSICAL RESEARCH, VOL. 91, NO. C11, PAGES 12,899–12,918, NOVEMBER 15, 1986

Mesoscale Hydrographic Variability in the Vicinity of Points Conception and Arguello During April–May 1983: The OPUS 1983 Experiment

LARRY P. ATKINSON,[1] KENNETH H. BRINK,[2] RUSS E. DAVIS,[3] BURTON H. JONES,[4] THERESA PALUSZKIEWICZ,[5] AND DAVID W. STUART[6]

In April and May 1983, interdisciplinary oceanographic observations were made of upwelling events in the Point Conception area off southern California. The principal objective was to observe the structure and time dependence of the upwelling system. To accomplish this, two ships, two aircraft, moorings, drogues, and satellite imagery were all included in the observational effort. During the intensive measurement period three main upwelling events and two intervening relaxation or downwelling intervals were sampled during what was a period of overall longer-term sea surface warming. Surface temperatures during upwelling were as low as 10.5°C in the upwelling center between Point Arguello and Point Conception, while during periods of nonupwelling winds, temperatures reached 14°–15°C in the same area. The upwelling center was also a source of higher-salinity water (33.7‰) relative to the offshore waters that were anomalously fresh (33.3‰). Upwelling was observed off Point Arguello, Point Conception, and the area between with a possible lag of up to a day at Point Conception relative to the other areas. The upwelling plume as observed by surface mapping and remote sensing tended to move in a variety of directions from SE to SW. Part of the movement was usually into the Santa Barbara Channel, but other parts of the plume occasionally moved southwestward. There was no obvious correlation of plume direction with the wind. During relaxation events the entire region was covered by a 10- to 20-m-thick warm (14°–16°C), fresh (< 33.5‰) buoyant layer. Spatial correlations of water temperature with 24-hour lagged winds showed logical patterns, but the distributions were not as seen in other California studies.

1. INTRODUCTION

Wind-related upwelling along the west coast of North and South America has been observed and studied for many years, creating a large body of knowledge on the physical, chemical, and biological dynamics of these systems at a variety of temporal and spatial scales. With the advent of satellite technology in the 1970s it became apparent that these upwelling processes were more spatially complicated than was originally envisioned, and a new appreciation was gained for the effect of topographic features such as capes and points and of major changes in the direction of the coastline. Such topographic effects had been previously observed along such areas as the California coast [*Sverdrup*, 1938; *Reid*, 1965], but we now, because of these new technologies, had a large-scale synoptic view of the systems. Along the central and northern California coast, jets and eddies are now well known [*Mooers and Robinson*, 1984; *Kelly*, 1983; *Traganza et al.*, 1980; *Breaker and Gilliland*, 1981; *Rienecker et al.*, 1985; *Davis*, 1985].

The Organization of Persistent Upwelling Structures (OPUS) program was designed to synoptically study the physics and biology of such localized upwelling systems. The area between points Arguello and Conception was chosen for the study because enhanced upwelling has been previously observed there [*Reid*, 1965; *Breaker and Gilliland*, 1981]. In the spring of 1981 a pilot observational program was conducted in the area, and the results have since been reported [*Brink et al.*, 1984; *Jones et al.*, 1983]. The scientific findings indicated that there was considerable topographically induced structure in the near-surface winds and that upwelling was enhanced in the region of the points. The evidence suggested that the winds were not entirely the cause of the upwelling. An important observation was sea surface temperature (SST) and nutrient patchiness on scales of 5–15 km.

Point Arguello marks the southern extent of the north-south trending California coastline, south of which the coast trends southeast towards Point Conception and then eastward into the southern California basin (Figure 1). Isobaths shallower than 500 m tend to follow the coastline, but deeper isobaths continue on a trend southeast; thus there is a divergence in isobaths above about 500 m. The Santa Barbara basin is isolated by a 500-m sill extending southward from Point Conception. *Emery* [1960] provides a good discussion of the geological features of the area. The distance between points Arguello and Conception is about 20 km and is useful for comparing figures.

Our purpose here is to describe the general mesoscale hydrographic variability that we observed in the Points Arguello and Conception during the OPUS 83 observational experiments and thus to serve as an introduction to more detailed papers on specific topics.

2. OBSERVATIONAL RATIONALE AND PLAN

The observational plan was based on the goal of obtaining data over a sufficiently large area around points Arguello and Conception to define the spatial structures with sufficient synopticity and resolution to provide accurate maps representing temporal changes. These goals were met by utilizing two ships, one to map rapidly (the R/V *New Horizon*) and one to make more time-consuming biological rate measurements (the R/V *Velero IV*); aircraft (the National Center for Atmospheric Research (NCAR) Queen Air for thermal IR and wind and the Scripps Institution of Oceanography aircraft for drogue tracking); and satellites. The area over which these observations were made is shown in Figure 1.

[1]Department of Oceanography, Old Dominion University, Norfolk, Virginia.
[2]Woods Hole Oceanographic Institution, Woods Hole, Massachusetts.
[3]Scripps Institution of Oceanography, La Jolla, California.
[4]Department of Biological Sciences, University of Southern California, Los Angeles.
[5]School of Oceanography, Oregon State University, Corvallis.
[6]Department of Meteorology, Florida State University, Tallahasse.

Paper number 6C0358.
0148-0227/86/006C-0358$05.00

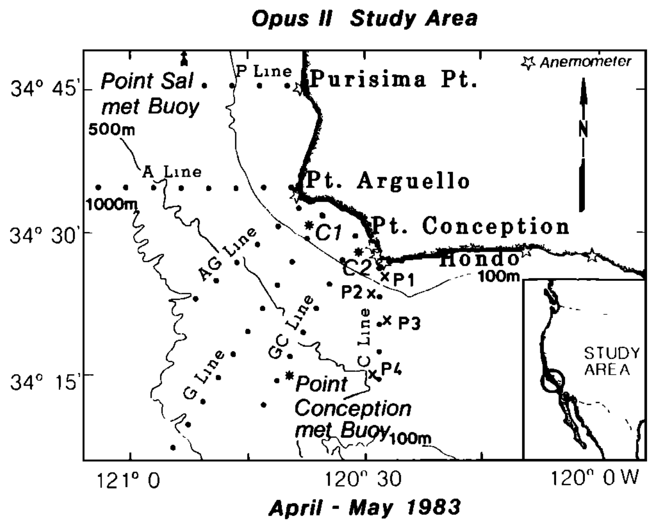

Fig. 1. Observational area showing meteorological moorings and land stations, current meter moorings, and cruise tracks. The AG and GC lines were sampled during mapping. C1, C2, and P1–P4 are current meter locations.

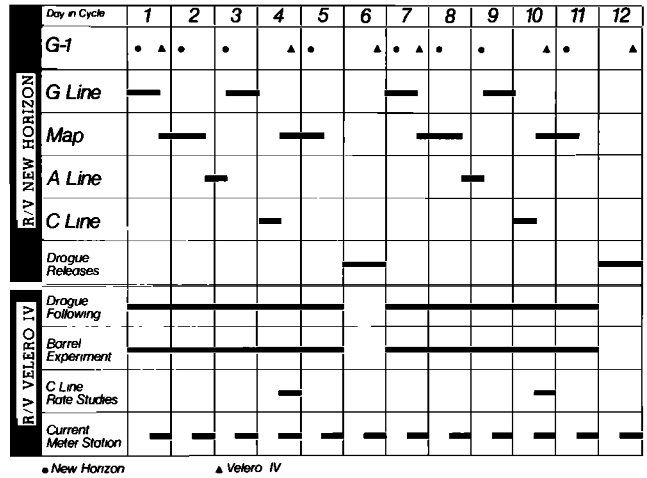

Fig. 3. Sampling sequence. The bars, triangles, and dots indicate when a particular station or section or the area was sampled.

The schedule of observations was designed to satisfy many, often conflicting, criteria, as follows (refer to Figure 1 for station locations):

1. Station G-1, between points Arguello and Conception, should be sampled by conductivity, temperature, and depth probe (CTD) every 24 hours. The G-1 station was assumed to be positioned in the upwelling center [see *Brink et al.*, 1984].

2. The G line, extending offshore between points Arguello and Conception, should be sampled by CTD every 2–3 days. The G line was assumed to lie along the axis of the upwelling center. In fact, it was sampled for temperature (by expendable bathythermograph (XBT) or CTD) every 1.5 days.

3. The whole area should be mapped every 2–3 days. The wind events occurred typically at 4- to 8-day intervals; thus it was desirable to map the affected area at least twice during that period. The mapping would entail surface measurements, XBTs, limited CTDs, and Doppler log current meter measurements.

4. Drogues should be deployed in the area to define flow in the upwelling center and to aid in biological sampling.

The resulting schedule, which is shown in Figures 2 and 3, gives the time period over which the observations were made and the frequency with which they were made. The ships operated on a 12-day cycle to allow port calls. Subsequent analysis, such as that reported here, suggests that the observational plan adequately sampled the system. It should be noted that subsequent analysis showed that synoptic scale wind field variability was 2–8 days (see section 4).

The sampling area (Figure 1) extended from Hondo in the Santa Barbara Channel to the east, swept around points Arguello and Conception, and extended north to Purisima Point. The area of more intensive sampling was between Point Conception on the east and straight west of Point Arguello to the north. The observations extended across the full width of the western end of the Santa Barbara Channel, and to the west of the channel, observations were extended up to 56 km (30 miles) offshore. No measurements were made between or south of the Channel Islands. This intensive area was selected based on the examination of data obtained during the 1981 OPUS experiment and satellite-derived thermal images. All shipboard, aircraft and drogue experiments were carried out in the Point Arguello–Point Conception area with the satellite providing coverage over the larger area. In addition to moving

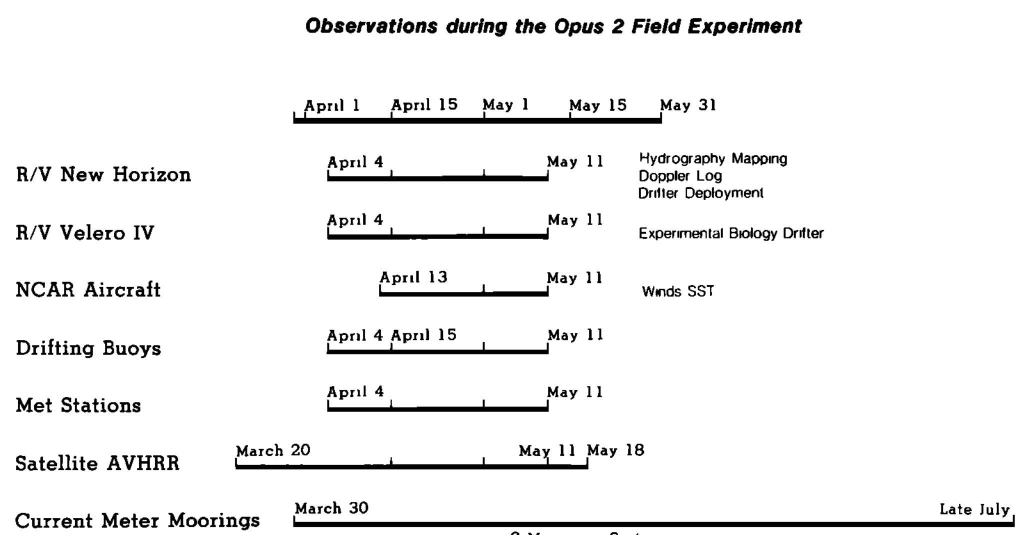

Fig. 2. Time line of various sampling operations.

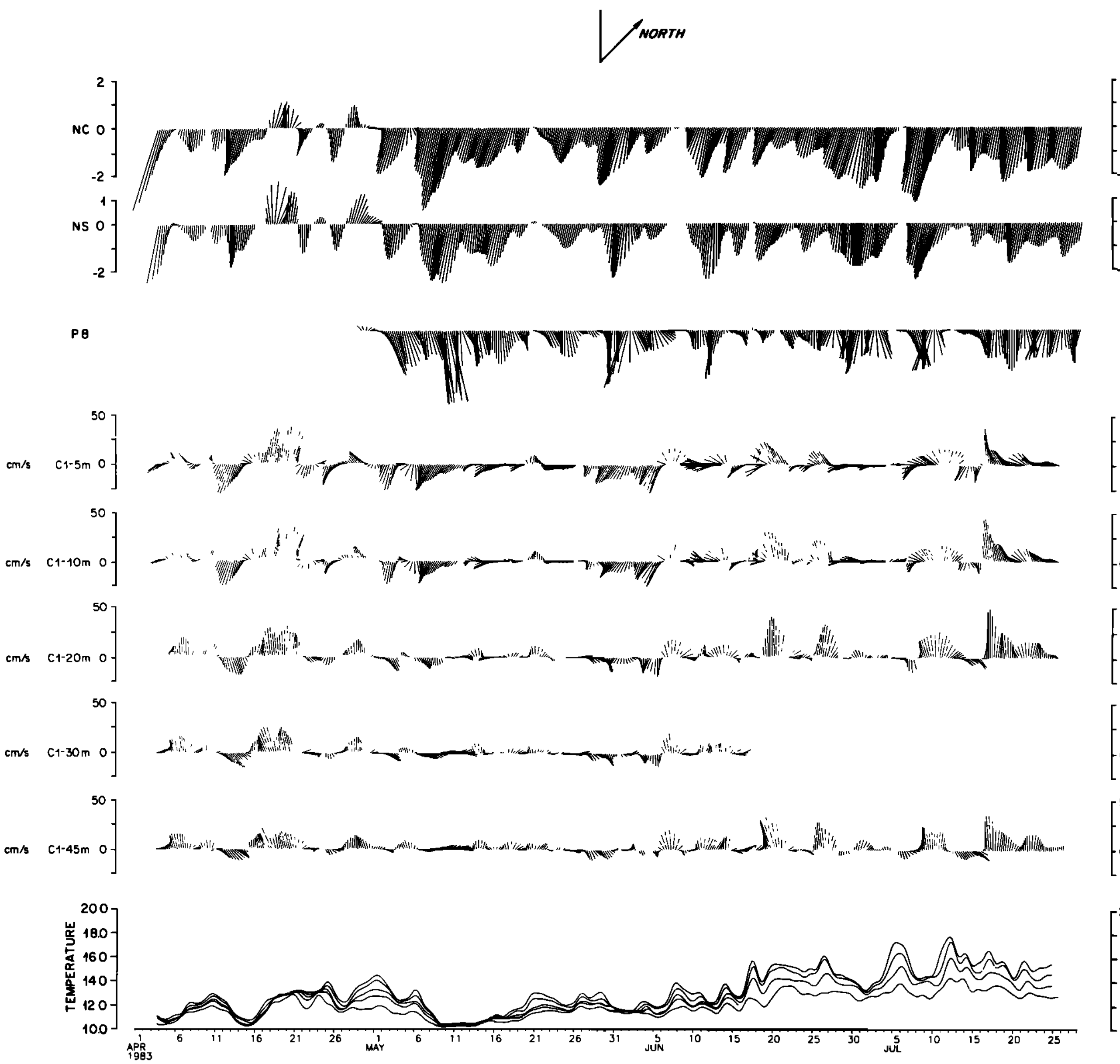

Fig. 4. Low pass-filtered wind stress from the Point Sal buoy and temperature at 5, 10, 20, 30, and 45 m from mooring C1. Winds are rotated 45° into the local alongshore direction.

platforms, current meters were moored between points Arguello and Conception, and shore meteorological stations were established for the duration of OPUS 83 [*Brink and Muench*, 1986; *Caldwell et al.*, 1986]. A valuable addition to the OPUS 83 data set was provided by the Minerals Management Service program in the Santa Barbara Channel conducted by Science Applications International, Inc., and Dynalysis of Princeton. They placed current meter moorings across the channel south of Point Conception (Figure 1), among other places. They also conducted a hydrographic survey of the channel east of Point Conception during our study period (J. T. Gunn, personal communication, 1985).

3. The Seasonal Setting

Southward winds intensify and become more persistent in the study area during the spring, resulting in a tendency for enhanced upwelling [*Enfield and Allen*, 1980; *Hickey*, 1979]. However, at the same time, solar heating is increasing, causing

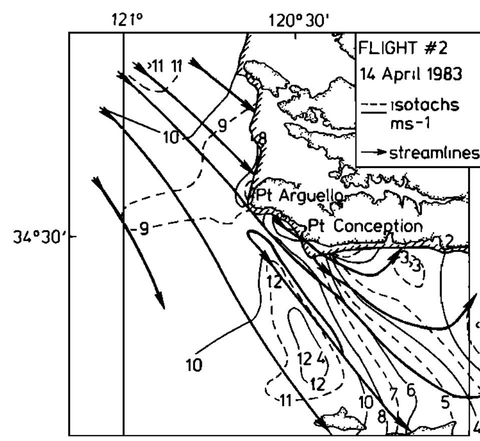

Fig. 5. Flight level winds at 152 m (500 feet) showing stream lines and isotachs during upwelling favorable winds. Note the wind speed maximum south of Point Conception and the wind speed gradient between there and the coast.

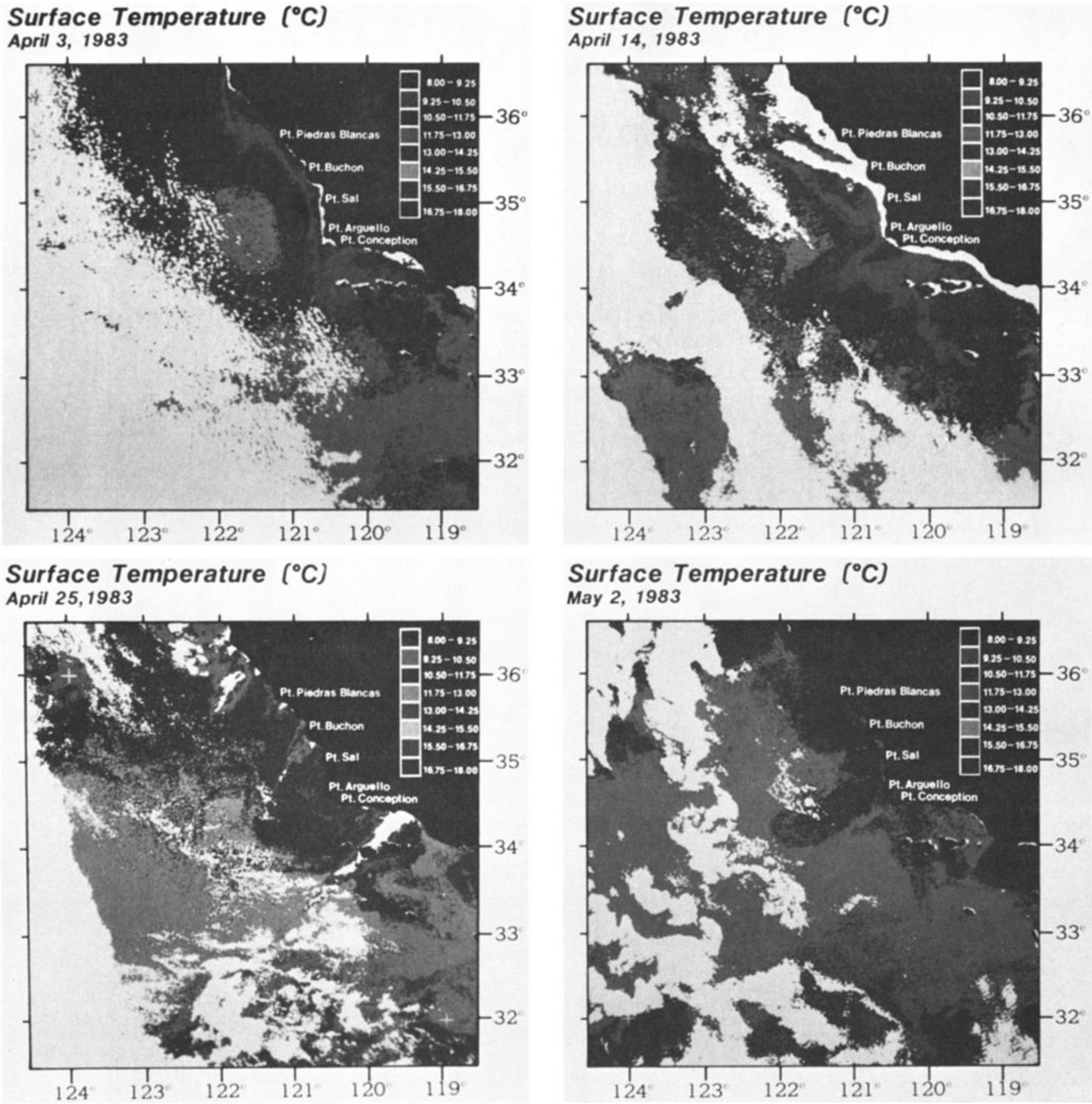

Plate 1. Surface temperature from the NOAA 7 AVHRR. The mean and variance of the temperatures are also shown. The data are valid around the Point Arguello–Point Conception area and are less valid elsewhere because of clouds. Thus the reader should focus mainly on the upwelling plume extending from the points and less on offshore structures and features along the coast north of Point Arguello unless it is specifically mentioned in the text. The statistics in the vicinity of the plume are valid, but those along the north coast and in the western and southwest portion of the images are inaccurate. (The color version of this figure can be found in the separate color section in this issue.)

surface waters to warm and surface layer buoyancy to increase. The wind and temperature records (Figure 4) from the Point Arguello–Point Conception area during the time of our study [*Brink and Muench*, 1986] suggest that in April upwelling winds occurred but were not steady. Temperature records from current meters at 5–45 m show a warming trend through April with cooling events associated with upwelling periods. Seasonal warming is also evident in these data.

4. Wind Field Variability

The primary analysis of the wind field is contained in manuscripts by *Caldwell et al.* [1986] and L. W. Eddington et al. (unpublished manuscript, 1986). Their studies contain detailed descriptions of the climate, topographic features, and observed spatial and temporal variability of the wind field observations made from land stations, meteorological buoys, and from the NCAR aircraft.

The wind was measured at many points, but we will present the results from the Point Sal buoy, which is representative of the exposed part of the study area. The stress shown in Figure 4 is low-pass filtered with a half-power point of 47 hours. There were three principal wind events that were upwelling favorable: 2–5, April 10–16, and May 2–19, and there were two downwelling events: April 17–21 and April 27–30. The

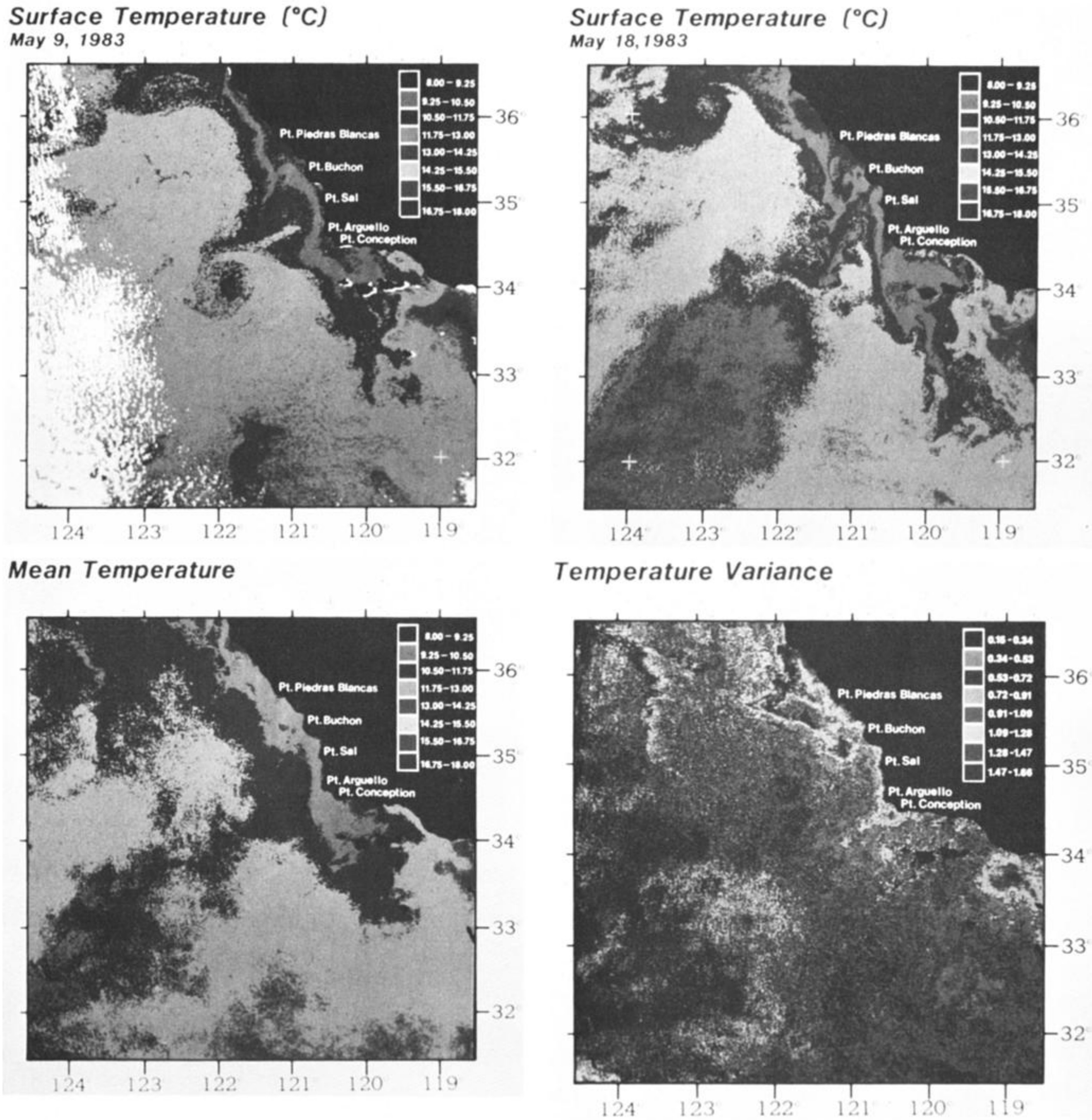

May 2–19 upwelling favorable wind event was interrupted by weak winds on May 5–6. The maximum stress during upwelling events was about 3 dyn cm^{-2}.

The spatial variability measured by the NCAR aircraft was considerable. During upwelling favorable winds the stream lines were from northwest to southeast with a velocity maximum south of Point Conception (Figure 5 is typical). Minimum velocities were observed in the lee of the mainland both in the mean and during individual events. The speed gradient from the lee of Point Conception to the speed maximum was about 0.5 m s^{-1} km^{-1} (stress gradient = 0.45 dyn cm^{-2} km^{-1}) at 152 m above sea level. The speed maximum is caused by local variations in the marine boundary layer height that are in turn affected by the Arguello headlands [L. W. Eddington et al., unpublished manuscript, 1986). Spectral analysis indicated synoptic scale events with periods of 2 and 4–5 days in April and 8 days in May [*Caldwell et al.*, 1986]. The mean flow and the 2- to 5-day variability were greater at the exposed buoys and coastal towers than in the protected locations bordering the Santa Barbara Channel. Diurnal wind variations were observed at both the Point Sal and Point Conception meteorological buoys, with the effect decreasing with distance offshore. The greatest sea breeze effect was observed at coastal stations along the north shore of the Santa Barbara Channel.

5. VARIABILITY AS INFERRED FROM SURFACE FIELDS

Previous observations in the Point Arguello–Point Conception area [*Brink et al.*, 1984] and the present data show a

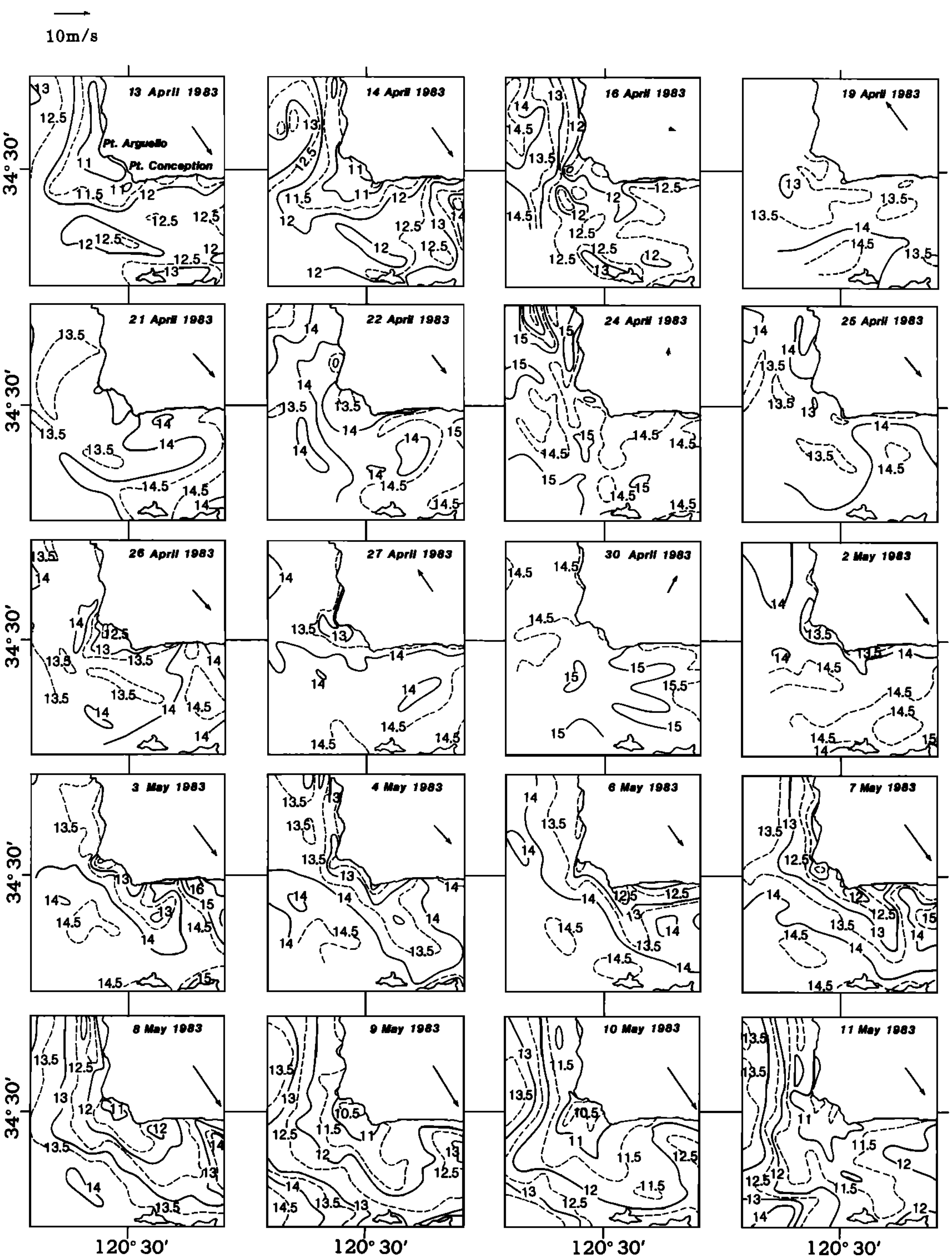

Fig. 6. Sea surface temperature maps from the NCAR aircraft flights. Dates of the flights are indicated. The data were obtained with a standard precision radiation thermometer. The direction and strength of the daily averaged wind speed from the Point Sal buoy are denoted by an arrow over the land.

three-dimensional time-dependent field varying in response to wind and remote forcing. To begin describing the complex variability observed in 1983, we consider the sea surface temperature field as observed by satellite infrared imagery and by the NCAR aircraft, the surface salinity field, and tracks of surface drogues. The discussion also refers to the current meter data presented by *Brink and Muench* [1986], *Brink et al.* [1985], and J. A. Barth and K. H. Brink (unpublished manuscript, 1986). The exposition is arranged as a chronological narrative. We chose not to present the shipboard observations of surface temperature because they are spatially much poorer in quality compared to the satellite and aircraft IR observations. Surface density observations are not shown because they were reflected adequately in the surface temperature field. Dynamic topography was calculated but not shown because the choice of integration depth and of integration method [*Helland-Hansen*, 1934; *Reid and Mantyla*, 1976] affected the results to such a degree as to make them meaningless.

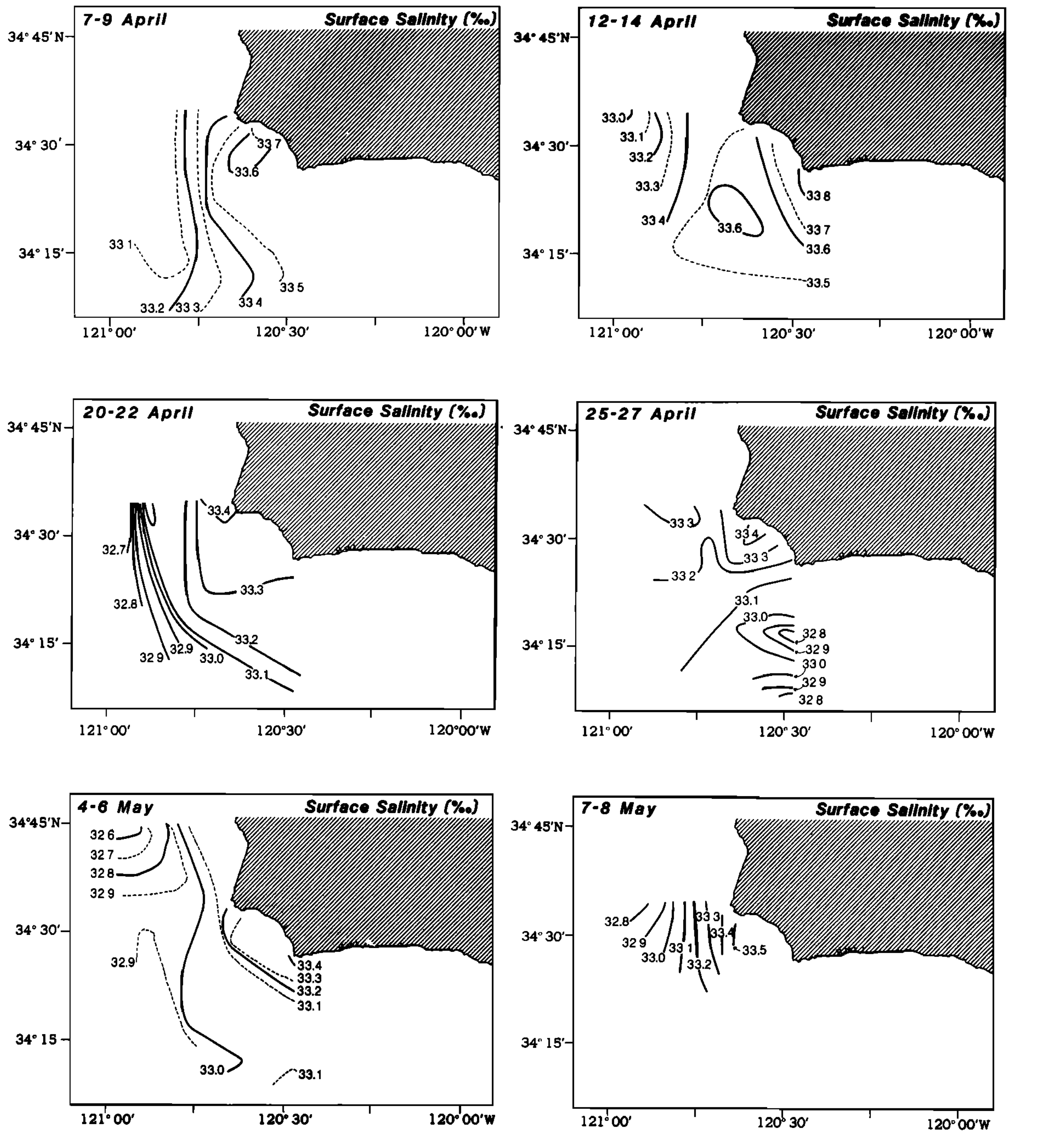

Fig. 7. Surface salinity maps obtained during CTD and XBT mapping runs. These maps contain data from the C, G, and A lines; the 4–6 May map also contains P line data.

The observations are presented in Plate 1 and in Figures 6 through 8. (Plate 1 is shown here in black and white. The color version can be found in the separate color section in this issue.) Plate 1 is a sequence of NOAA 7 infrared SST advanced very high resolution radiometer (AVHRR) images processed at the Scripps Satellite Oceanography Facility with software developed at the University of Miami using the *McClain et al.* [1983] algorithm and enhanced at the NASA Goddard Space Flight Center. These show the large-scale features around the area of focus and allow some inference of the surface flow field. Figure 6 is a sequence of SST maps from NCAR aircraft; these show more detail in the study area. Figure 7 is a sequence of surface salinity maps derived from CTD observations along the A, G, and C lines. While these salinity maps lack the synopticity and resolution of the SST maps, they are very helpful in identifying intrusions of water into the study region from the west, where both warm and cold eddies were found, and from the Santa Barbara Channel to the east. Figure 8 presents tracks from a fraction of the 72 drifters deployed to follow currents at 0.5-m depth. The technique is described by *Davis et al.* [1982] and additional data are presented by *Davis and Regier* [1984]. These tracks confirmed the flow patterns inferred from the SST and salinity fields. Nineteen additional drifters drogued to 25-m and 50-m depths were also tracked; these show a strong similarity to the surface drifters. Additional confirmation of the scenario developed here is provided by the hydrographic and current meter data presented in subsequent sections.

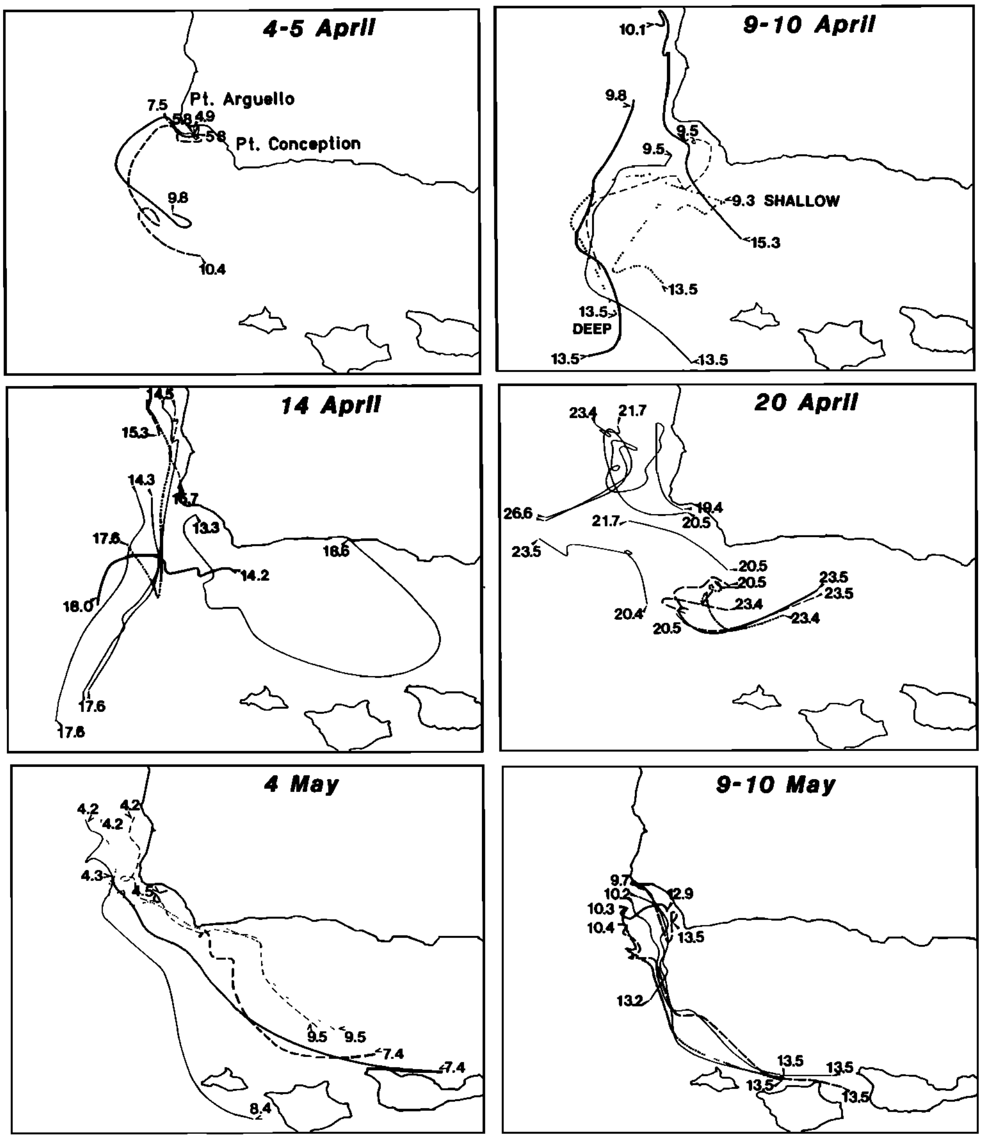

Fig. 8. Surface drifter tracks Labels refer to day and decimal day (e.g., 13.2 = April 13, 0500). Dates on panels are deployment dates. Times are PST.

5.1. *The April 3 Upwelling Event*

The April 2–4 event was characterized by strong upwelling favorable winds (Figure 4). The satellite image Plate 1 showed a band of cold water along the coast north of Point Arguello. Also evident was a cold plume originating between points Arguello and Conception, extending southward and spreading into the Santa Barbara Channel and between the Channel Islands. A warm eddylike feature was seen 50 km west of Point Arguello, and the warmest waters were offshore and to the south. Salinity maps taken later on April 7–9 (Figure 7) showed a local salinity maximum (33.7‰) between the points. This is a common feature during upwelling, since salinity increases with depth and the region between the points is apparently an upwelling center where these waters surface preferentially. Salinities were relatively constant in the channel (33.5‰), and low salinities (<33.1‰) were found in the northwest.

The distribution of SST and salinity suggests that strong upwelling was occurring between the points where there was offshore advection, that there was upwelling (or advection of upwelled water) along the coast north of Point Arguello, and that there was advection eastward into the southern part of the Santa Barbara Channel. The surface drifters deployed April 4–5 and tracked until April 10 confirm an offshore and then eastward drift (Figure 8).

Winds during April 6–11 were weakly upwelling favorable. Drifters deployed on April 6 (not shown) behaved similarly to the April 4 deployment but with stronger southward flow (20 cm s^{-1}) which carried buoys from between the points past the westwardmost island in 2.5 days. The drifters deployed April 9 showed the same general pattern: strong southward flow past Point Arguello and generally southwestward motion of water from between the points. Westward flow past Point Conception led to a confluence between the points followed by drift southward past the islands.

5.2. *The April 12–14 Upwelling Event*

Strong upwelling favorable winds occurred during April 12–14 and were followed by weaker winds until April 17. In the April 13 aircraft SST (Figure 6), upwelling between the

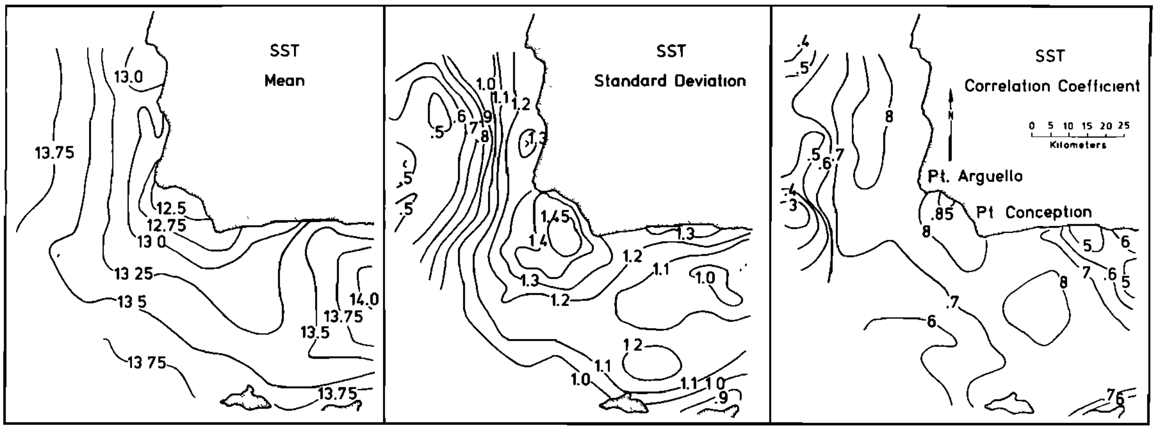

Fig. 9. Mean and standard deviation of the aircraft SST field using all data shown in Figure 6 except those of April 19. The wind-temperature correlation is also included. See text.

points was clear, as was some upwelling north of Point Arguello. Warm water from the apparent offshore eddy identified above appeared as a lobe of 13.0°C water intruding from the west.

In the April 14 aircraft and satellite maps, warm water from the channel had advanced into the far eastern part of the study area. A large region of cold water between the points evidenced continued upwelling, but compared with the satellite image of April 3, the plume orientation had shifted to the southwest and cold water extended farther into the Santa Barbara Channel. The warm water from the Channel and the southwestward shift of the plume were presumably the result of the westward flow past Point Conception seen in the April 9 drifter tracks. The SST patterns in the vicinity of the apparent offshore eddy suggest that this feature entrained upwelled water and influenced the plume orientation. This feature appears in the April 12–14 salinity maps as values as low as 32.9‰. The highest salinity (33.8‰ higher than any value in the previous map) was found intruding from the channel past Point Conception, evidently advected by the westward flow there or from localized upwelling just east of Point Conception.

The drifters deployed on April 14 showed continued southward flow past Point Arguello after winds from the north ceased. Nearshore westward flow past Point Conception persisted while three buoys (one shown) traveled from the study area eastward into the southern channel and then were entrained into westward flow in the northern channel. Judging from various complicated and crossing trajectories (two shown), the confluence of southward and nearshore westward flow between the points was chaotic and time dependent. The April 16 aircraft SST chart shows that the warm water had completely obliterated the upwelling plume.

5.3. *The April 17 Through May 1 Downwelling and Relaxation Period*

There were strong downwelling winds during April 17–20 and weaker and variable winds until May 1. Satellite images during this period were degraded by clouds but do suggest that the cold water along the coast spread westward with warmer water found offshore in the south and in the eastern Santa Barbara Channel. The warmest water was found along the coast east of 119°W. The April 25 image shows this and the continued warming of the region. The patchiness may indicate the breakup of the previous plume. The apparent warm eddy west of Point Arguello was no longer evident. The time variation was consistent with onshore and northward advection of formerly offshore warm water during this relaxation period.

Prior to the April 16 aircraft survey the wind slackened and temperatures in the upwelling center increased with the warmest water found to the west. Even during the April 17–20 downwelling favorable winds, the aircraft surveys show the coldest water to be between points Arguello and Conception. On April 26 there was a brief period of upwelling favorable wind, and colder water appeared between the points. Note that the plume apparently extended southwestward during this brief event.

The surface salinity map of April 20–22, during and immediately following the downwelling event, shows depressed salinities at all locations. The highest salinities (33.4‰) were found just north of Point Arguello, with salinity decreasing strongly to the west (to 32.6‰), perhaps associated with the offshore eddy, and generally low salinity (33.1‰) found in the southern channel. In the April 25–27 survey, toward the end of the wind relaxation period, the salinity pattern was less coherent but high salinity water remained near Point Arguello, with a trend of decreasing salinity toward the southern channel. The largest change between these surveys was the decrease of salinity to 32.7‰ in the southern channel.

Drifter tracks from April 14–17 suggested a general pattern of continuing southward flow past Point Arguello and westward flow past Point Conception forming a plume which moved southwestward then southward and then either continued southward without entering the channel or turned eastward and flowed into the southern channel. By April 21, following the downwelling event, the flow past Point Arguello was variable and weak with a bias (from all drifters, some not shown) toward the north. In contrast to this change in the flow past Point Arguello, flow past Point Conception continued to be westward along the shore and eastward in the southern channel.

5.4. *The May 2–18 Upwelling Period*

The period from May 2 through May 6 was characterized by light upwelling favorable winds, and the period from May 7 through May 17, by sustained strong upwelling favorable winds.

In the satellite image of May 2 the coldest water appeared southeast of points Arguello and Conception as upwelling commenced. Warm water was still evident in the channel, and even warmer water was seen to the south and east. The apparent warm eddy west of Point Arguello was not detectable, and instead cold water extended west-southwest to 123°W from Point Arguello, possibly a remnant of the previous upwelling plume. By May 9, at the peak of the upwelling favorable winds, larger regions of cold water developed around the points. The upwelling plume was evident to the southeast, extending into the channel and between the Channel Islands. The plume also extended southwest from Point Arguello and appeared to be entrained by a cyclonic cold eddy. Regions of warm water were found between the two plumes, offshore, and along the coast to the east.

The aircraft surveys from April 30 through May 11 show the temporal evolution of the upwelling plumes with great clarity. Downwelling favorable winds and warm temperatures dominated until May 2, when the coldest water was found around both points. Cooling along the coast north of Point Arguello suggested upwelling in this region as well. This picture intensified during May 3–4, with the upwelling plume growing to the southeast. In the channel east of Point Conception, temperatures increased, probably indicating continued westward advection in the northern channel. Winds abated briefly on May 5 and then increased on May 7. During this period, nearshore temperatures continued to decrease and the plume appeared to spread along the coast into the channel. On May 7, warm water appeared to have advanced westward in the central channel, perhaps in response to increasing southward winds. *Brink and Muench* [1986, Figure 7] noted that a westward jet in the channel was common but weakened during the first part of the May wind event and then was reestablished before the event abated. During May 8–11 the plume developed further, with the temperature of the coldest water, between the points, decreasing to 10.5°C by May 10. The plume expanded further to the southeast and also penetrated to the southwest, as was evident in the satellite image from May 9. By May 11 the plume dominated almost the entire aircraft survey area except the southwest quadrant, where a lobe of warm water was found between the plume and the apparent offshore cold eddy (see also the May 9 satellite image).

In the May 4–6 survey, during the start of the intense upwelling event, surface salinities were greatest between the points and along the north shore of the channel. This was the region of cold water, consistent with active upwelling which brings high-salinity water to the surface. Low salinities were found to the northwest and southwest of Point Arguello, with the lowest salinities to the northwest. This is a region of high surface temperature, although there was not a tight T-S relation. In the May 7–8 survey, near the peak of the wind forcing, increased salinity was found between the points and low salinities remained to the west of Point Arguello.

The drifters deployed on May 4 were tracked during the peak of the upwelling period. The pattern was simple, with flow southward past Point Arguello turning southeastward and primarily entering the channel along the southern side. Speeds averaged 35 cm s^{-1} over 3 days, and three drifters were observed to pass through the channel to the east. This pattern differed substantially from those observed in April, all of which showed evidence of westward flow along the northern edge of the channel past Point Conception. There may have been westward flow in the northern channel in May, but it did not penetrate to Point Conception and it did not entrain water from the southern channel as was observed in the April 14 and 20 deployments. The drifters deployed May 9 showed a similar pattern with a tendency for drifters to hug the southern channel boundary and even penetrate between the islands.

By May 18, winds had been strong and upwelling favorable for over 2 weeks. In the May 18 satellite image the regions of cold upwelled water had spread south and southeast, extending through the islands, as was suggested by the track of the May 9 drifters. But despite strong southeastward winds, warm water was still found along the mainland coast in the channel. The apparent offshore cold eddy was no longer evident, but it may have been obscured by clouds.

It is interesting to compare the April 3 and May 18 satellite images, both of which followed upwelling events. The general distributions are similar and suggest the importance of large-scale advection and the influences of entrainment into eddies. The plumes in all of the upwelling images are similar in character to the filaments observed farther north by *Rienecker et al.* [1985] in an area of quite different coastline topography.

5.5. *Summary*

The observation period consisted of three regimes: (1) an upwelling period from April 2 through April 16, (2) a downwelling and weak wind period from April 17 through May 1, and (3) a strong upwelling period from May 2 through May 19. While each of the observed fields exhibits unique complexity, there are recurrent patterns in each and in the relation between them.

The mean and standard deviation in the aircraft SST are shown in Figure 9, and the mean and variance in the satellite SST measurements are shown in Plate 1. In the mean, the coldest temperatures were found along the coast from just north of Point Arguello to just east of Point Conception, outlining the regions of apparent upwelling in the individual images. The coldest mean temperature in the aircraft measurements was 12.2°C at a point on the east side of Point Arguello. The cold plume extended southward and eastward into the channel, and in the aircraft mean SST map, the plume appeared also to extend southwest. The southeastward trend follows the typical path of drifters released in the region between the points. Warm water extended along the northern channel shore from the east. Highest variability was observed in the area of the plume, with maximum values in the aircraft SST maps of 1.49°C at a point 10 km offshore between the points. North of Point Arguello and east of Point Conception, standard deviations were highest along the coast and decreased offshore in mild contrast to the situation between the points. Variability was least in the area west of Point Arguello that was under the influence of the warm, low-salinity offshore water.

In general terms, the drifter tracks indicate three current elements which affect the advection of SST and surface salinity. West of Point Arguello there was typically southward flow, more or less the "terminus" of the current along the north-south coastline. In the northern channel the flow was primarily to the west, toward the upwelling center. In the southern channel, flow was toward the east, counter to the flow along the northern shore. In early April, westward flow past Point Conception was strong, and this may have forced the upwelled plume in the confluence between the southward and eastward flows to initially move southwestward and to generally pass southward without entering the channel. In the later upwelling periods the northern shore westward flow did not penetrate past Point Conception, and flow from between the points largely entered the southern channel. During the downwelling period the flow past Point Arguello weakened or reversed, while the westward flow past Point Conception expanded to include much of the western channel entrance.

Other conclusions can be drawn from examination of the collection of individual surface observations. The coldest upwelled water was consistently found between the points. The

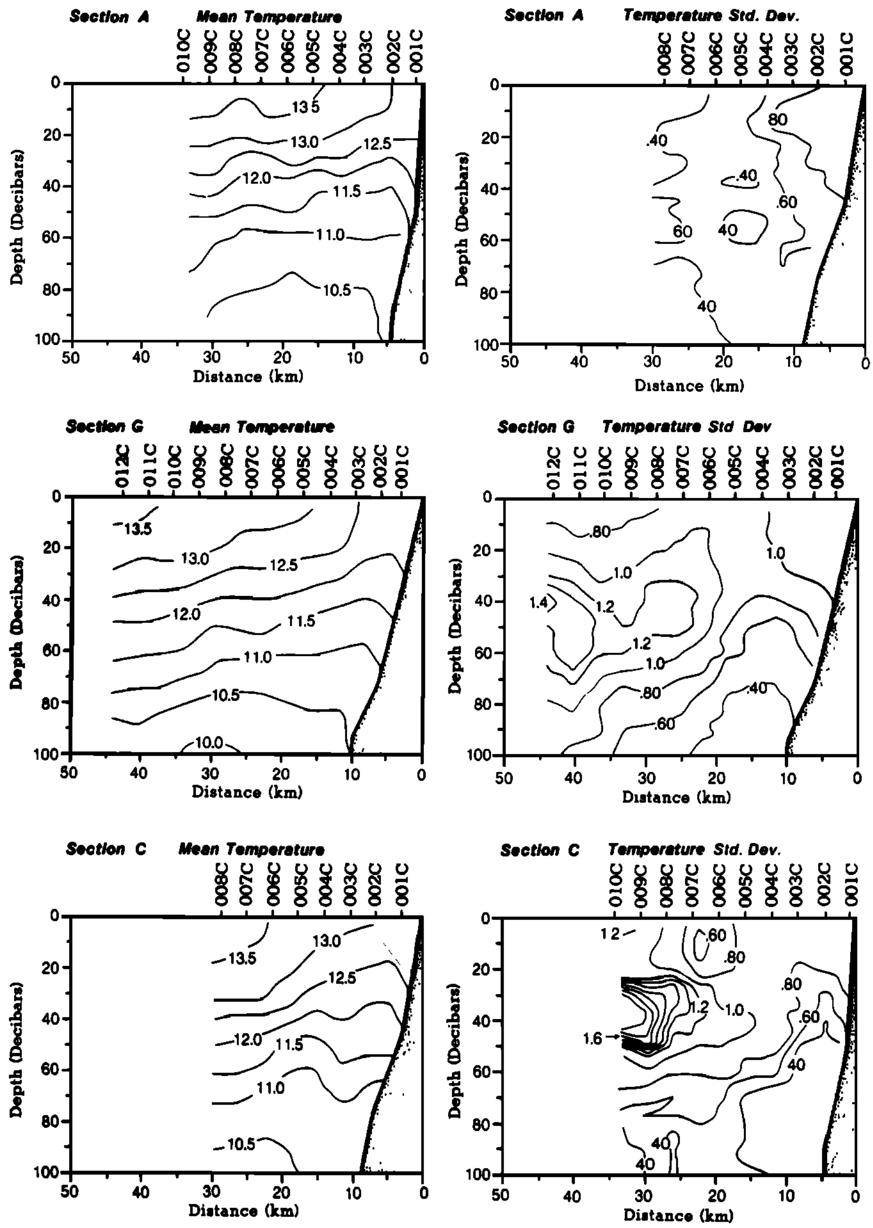

Fig. 10. Mean and standard deviation in the temperature field on the A, G, and C lines. The number of samples is 15, 22, and 15, respectively.

high salinity of these waters was an additional indicator of upwelling. A mass of warm, low-salinity water persisted to the west of Point Arguello. The upwelling plumes, as is indicated by SST, salinity, and drifter tracks, extended offshore from near Point Arguello in different directions under similar wind conditions. During the April upwelling period the plume extended southwest, then south, whereas in May it trended south, then southeastward through the southern channel and Channel Islands. Offshore eddies, first warm anticyclonic and then cold cyclonic, apparently affected adjacent waters by entraining coastal waters and provided a source for warmer, buoyant offshore water intrusions into the upwelling area.

6. Variability as Inferred From the Subsurface Fields

The complexity of the surface field is reflected in the subsurface fields, but except for temperature, we have much fewer data, and less intense and synoptic data, than were available for the surface fields. Data to be examined will include the mean and standard deviation of temperature, salinity, and density along the three main hydrographic sections (Figures 10–12); the temperature, salinity, and density sections from the G line (Figures 13*a* and 13*b*); and the variability in temperature, salinity, and density at stations A-3, G-3, and C-3 (Figures 14–16).

6.1. *Mean and Variability in the Subsurface Temperature, Salinity, and Density Fields*

The mean temperature sections (Figure 10) were derived from CTD and XBT data, and all suggest upwelling, with isotherms in the upper 40–60 m generally rising towards the coast. Nitrate concentrations often increased to observable levels at 13.5°C; at lower temperatures nitrate concentrations were even higher. The G line appeared coldest, with the 12.5°C isotherm breaking the surface 10 km offshore. On the C and A lines the 12.5°C isotherm remained below 20 m. The

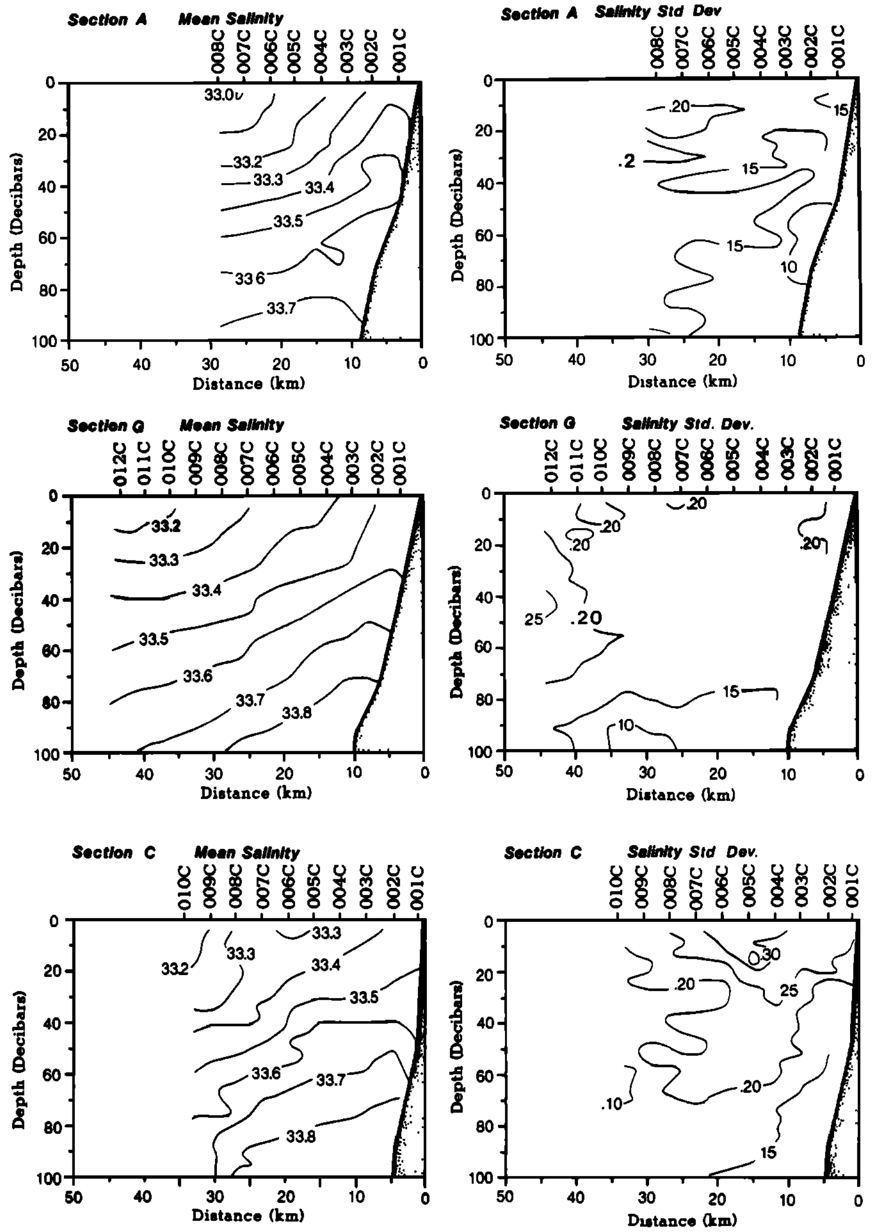

Fig. 11. Mean and standard deviation in the salinity field on the A, G, and C lines. The number of samples is 5, 13, and 5, respectively.

other isotherms also broke the surface further offshore along the G line, suggesting proximity to the axis of the mean cold plume, which is consistent with the mean SST maps. In all cases the isotherms within 5 km of the coast and below 20 m warped downward, suggestive of a poleward undercurrent.

Temperature standard deviation displayed two obvious maxima. One was observed in the inner part of the C and G lines near the surface, with values of 0.9°–1.1°C. This maximum was apparently associated with the upwelling center. The second maximum was observed in the outer part of the C and G lines, with values of greater than 1.7°C. This maximum was probably related to varying flow in the channel [*Brink and Muench*, 1986]. The G line was generally most variable, possibly because that was the location of the upwelling plume and the plume direction was highly variable. The G line was also an area where waters from the A line or C line area met during upwelling or downwelling periods.

The mean salinity and density sections were derived from CTD data and thus were calculated from fewer data than were temperature sections. The mean salinity distributions (Figure 11), as with temperature, indicate the general ascent of isopleths towards the coast with some downwarping within 5 km of the coast. The lowest average salinities (<33.0‰) were found on the outer part of the A line, and highest mean salinities were found at depth inshore on the C line. The highest mean surface salinities were found nearshore on the G line coincident with the coldest mean surface temperatures.

The zone of highest salinity standard deviation (0.3‰) extended from surface to depth, sloping deeper offshore, along the C line. A second area of maximum standard deviation (0.25‰) was observed at 40 m at the outer station on the G line. Salinity standard deviation along the A line was notably low (<0.2‰). The areas of high standard deviation probably reflect the contrast between the upwelling high-salinity water and the invading warm, low-salinity water.

The distribution of mean density (Figure 12) again suggests

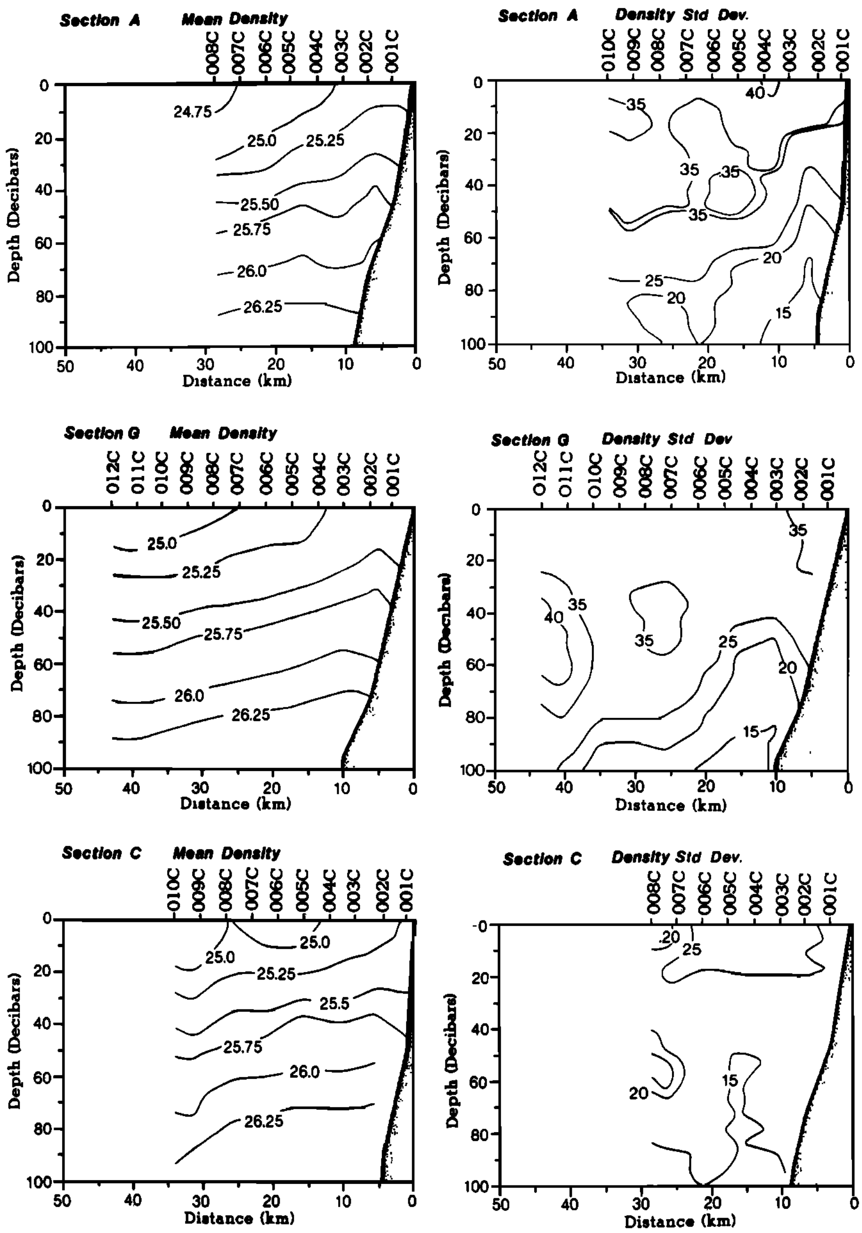

Fig. 12. Mean and standard deviation in the density field on the A, G, and C lines (σ_t units). The number of samples is 5, 13, and 5, respectively.

that the average condition was upwelling. The maximum standard deviation in the density field was in the C and G lines at both the surface and thermocline. As with temperature and salinity, the standard deviation was lowest along the A line. The complex structure of the density and salinity standard deviation is no doubt partly due the low number of samples and the relatively short period of the record.

6.2. *Vertical Structure Along the G Line*

The hydrography of the Point Arguello–Point Conception area is quite complicated, so to give an example of the time variability we will present the vertical sections from the G line (Figures 13*a* and 13*b*). The data presented are the vertical sections made from CTD data. No XBT sections are included, although they are part of the data set and were included in the previously discussed mean temperature fields.

When examining the variety of sections there are several persistent features to note: uplifting of isotherms associated with coastal upwelling, doming, downwelling, and intrusion of lighter water. Examples of typical upwelling can be seen on the April 5–6 and May 2–9 sections. In these sections, surfaces are sloped upward toward the coast above 100–200 m; below this the isopleths trend downward. From the thermal wind equation, this downward slope at depth suggests a deep poleward flow. Doming of isotherms was observed in sections on April 7–11. Our interpretation of this structure is that it represents a dome or ridge of formerly upwelled water that was isolated from the upwelling area nearer shore either by lateral advection or subsidence at the upwelling center near the coast. Either process probably begins after cessation of upwelling winds. Downwelling, which we interpret as a downward sloping of surfaces towards the coast, was observed in sections during April 11–26. In some cases, such as May 4–5, upwelling appeared to be occurring in the upper layer, but downwelling or a strong counterflow was occurring at depth. A warm and fresh buoyant layer was present offshore that was often ob-

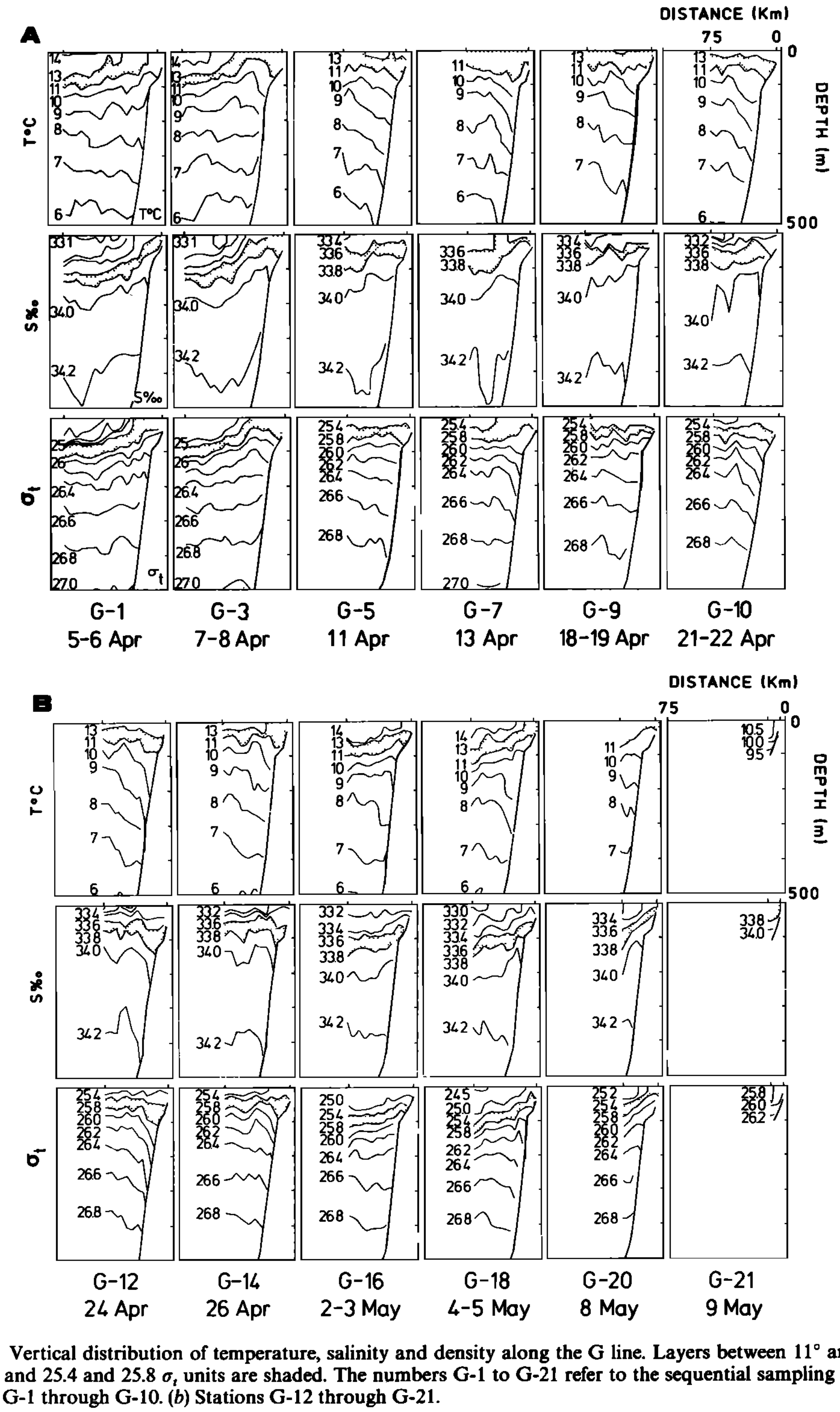

Fig. 13. Vertical distribution of temperature, salinity and density along the G line. Layers between 11° and 13°C, 33.6 and 33.8‰, and 25.4 and 25.8 σ_t units are shaded. The numbers G-1 to G-21 refer to the sequential sampling of the G line. (*a*) Stations G-1 through G-10. (*b*) Stations G-12 through G-21.

served during periods of downwelling and during the initial phases of upwelling before the resident buoyant surface waters had been advected from the area or buoyancy was altered via mixing.

The sections also show that during upwelling, offshore isopleths descended, while nearshore isopleths rose. Such features have also been observed by *Huyer* [1984], *Brink et al.* [1980], and *Breaker and Mooers* [1986]. The movement could be caused by advection, downwarping by heavier water moving offshore in the upwelling region, or mixed layer deepening offshore contrasted to upwelling nearshore.

A subjective analysis of all C, G, and A line sections, both XBT and CTD, was made to determine the approximate distribution between upwelling and downwelling conditions. The results were that upwelling was evident in 47%, 73%, and 53% of the A, G, and C lines, respectively. As in most of our observations, the G line was the center of upwelling activity.

6.3. *Variability on the A, G, and C Lines*

In Figures 14–16 the vertical time series of temperature, salinity, and density at stations A-3, G-3, and C-3 are shown. These stations were chosen to represent water within the zone of upwelling at locations west of Point Arguello (A-3), between the points (G-3), and south of Point Conception (C-3). The temperature data are more detailed because of the inclusion of XBT data.

At G-3 (Figure 15), which is normally near the upwelling center between the points, the three upwelling events that were noted in the wind and surface field are easily seen. On April 5 the water column was relatively well mixed with a deep surface layer of 11.0°–11.5°C water. The water was relatively salty (33.6–33.8‰). During a period of weak winds (April 6–11) the water column warmed, and the water in the region was fresher. It is interesting to note the depth (>45m) to which the

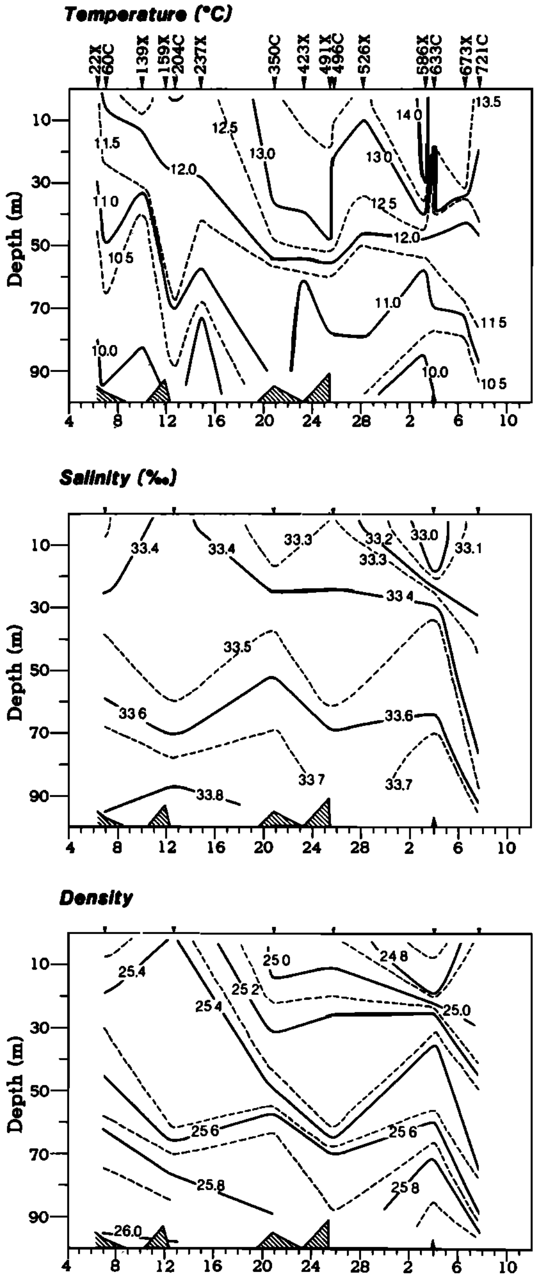

Fig. 14. Temperature, salinity, and density variations at station A-3. Time of sampling is indicated by the station numbers and tick marks at the top. A-3 is 10 km from shore. The cross-hatched area shows the bottom.

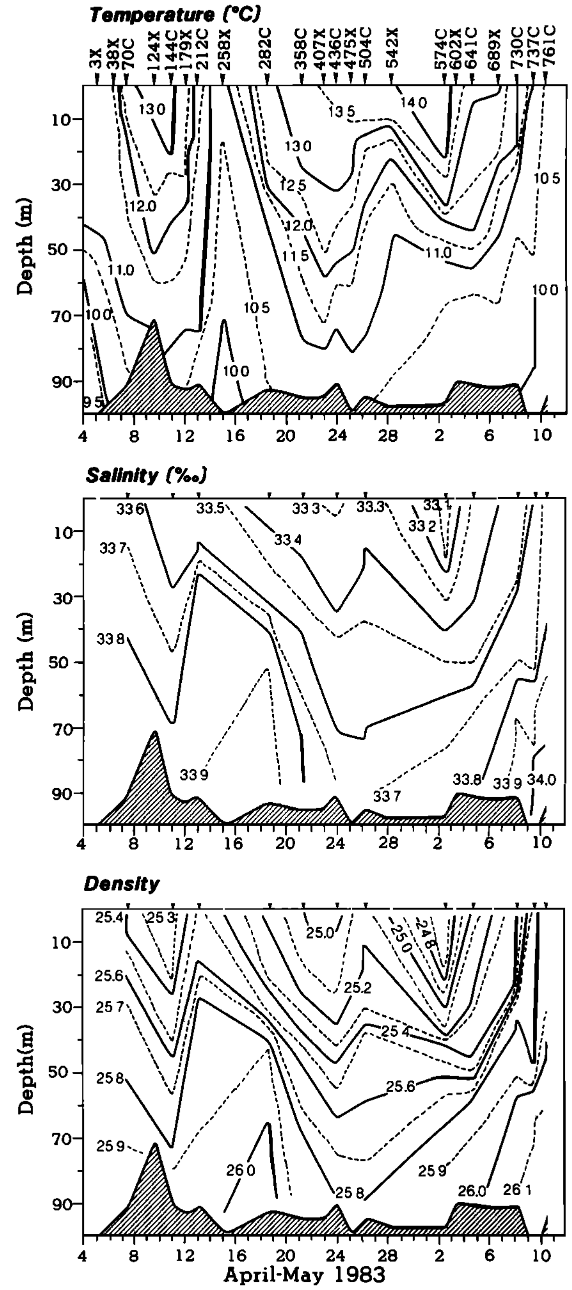

Fig. 15. Temperature, salinity and density variations at station G-3, 11 km from shore. The cross-hatched area shows the bottom.

warming was noticeable. This was deeper than what one would expect from warming via solar insolation and thus may indicate the role of advective processes. Wind stress magnitude increased, and the second upwelling event appeared to peak on April 15 with water between 10° and 10.5°C occupying much of the water column. Bottom salinity was slightly higher than before (33.9‰). Following that upwelling event, winds were weak and fluctuating, and we observed the impressive warming and freshening of the whole water column culminating in maximum temperatures of over 14°C and minimum salinities of less than 33.0‰. Note that the surface warming and freshening was out of phase with the bottom, where warming and freshening peaked on April 25, about a week ahead of the surface. The surface temperature fields suggest that this bottom layer warming and freshening was due to

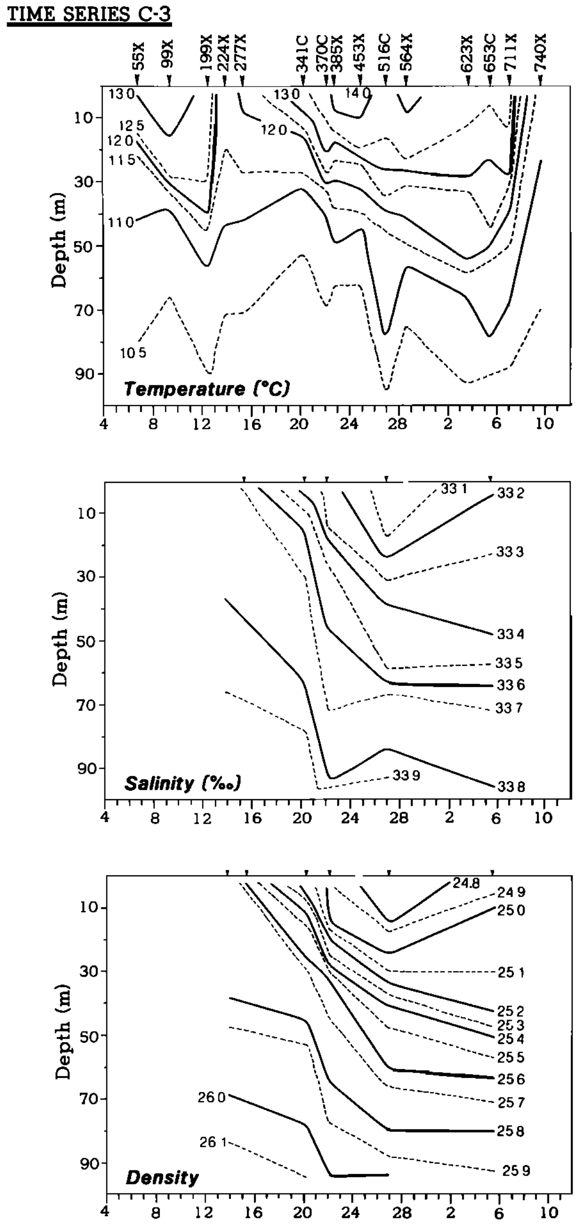

Fig. 16. Temperature, salinity and density variations at station C-3, 9 km from shore. The cross-hatched area shows the bottom.

an advection of offshore or southern waters. After the warming and freshening period the effect of the large upwelling event of early May was clearly observed. The water column rapidly cooled to <10.5°C and salinity increased to >33.7‰ at the surface and to <10°C and >34.0‰ at the bottom. Note that the upper layers responded to the upwelling event on about May 2, while the lower layers responded around May 3–7.

At C-3 (Figure 16), south of Point Conception and east of G-3, the situation was similar, with the three main upwelling events and the warming and freshening event being quite obvious. The deeper isotherms appeared to ascend before the shallower isotherms during the May event. This is consistent with the current meter observations [*Brink and Muench*, 1986]. Unfortunately, the final stations at C-3 were XBTs, so salinity data are not available. The isopycnals were generally continually deepening during the observation period but with some ascending above 70 m.

The A-3 time series, from west of Point Arguello, apparently reflects the effect of advective processes from the north and exhibits quite different characteristics. The early April and early May upwelling events are present, as is the April warming and freshening event, but the upwelling event that occurred on about April 14 is not obvious in the vertical structure. Possibly, the sampling missed it. During the first upwelling event in early April, temperatures were <11.3°C at the surface and <10.0°C at the bottom, nearly the same as at G-3. Salinities, however, were significantly lower in the upper layer (33.3‰ versus 33.6‰). With the warming and freshening, temperatures peaked at 13.1°C and salinity was as low as 32.93‰, quite similar to G-3. The upwelling event in early May, which was observed to start at G-3 on about May 2, was not obvious at A-3 until May 6. At A-3 the upper layer isotherms appeared to respond to the early May upwelling event, but the lower layer isotherms continued descending. In contrast to the time series at C-3 and G-3 the strong salinity changes were restricted to the upper 50 m until the May event, when the isohalines dipped sharply.

The initial conclusions that can be drawn from these observations are as follows: (1) The three major upwelling events were observed at the G and C line stations. The early April and early May upwelling events were observed at the A line stations, but the mid-April event was not seen there. (2) The C line station lagged the others by a few days. (3) The downwelling event of mid-April and late April caused the surface warming and freshening of the entire area with maximum effect observed on May 2 at locations G-3 and C-3 but later at A-3. (4) The upper layers usually responded to the upwelling favorable winds before the lower layers. (5) The vertical excursion of T, S, and σ_t surfaces often exceeded 80 m during upwelling events.

6.4. *Dependence of the Temperature Field on Wind and Time*

The temperature field structure and variability in upwelling zones often strongly depends on the wind field. To test this hypothesis here, we did two analyses. One analysis was to correlate the variability in the aircraft SST field with wind stress at the Point Sal buoy, and the second analysis was to correlate the variability in the temperature fields along the A, G, and C lines in a manner similar to that recently employed by *Huyer* [1984].

Winds for the wind-SST correlation were determined by averaging 25 wind stress values taken from the Point Sal buoy from 12 hours before until 12 hours after 0000 UT on the day of the specific flight. This effectively produces a 24-hour evenly weighted running average centered on the time when the aircraft flight was approximately half over. The true north component of the wind stress was used in the correlation. This is 45° to the right of the axis used in the following analysis. The results are comparable, since upwelling is related to southward winds in general.

The following procedure was used to determine the correlation between the vertical temperature field and the wind. For the regression analysis involving subsurface temperatures, we had to choose a representative time lag between winds and temperatures. This was not entirely straightforward, as is shown by empirical orthogonal function (EOF) analysis. Examples of the EOF structures used can be found in the work of *Brink and Muench* [1986]. The time series associated with

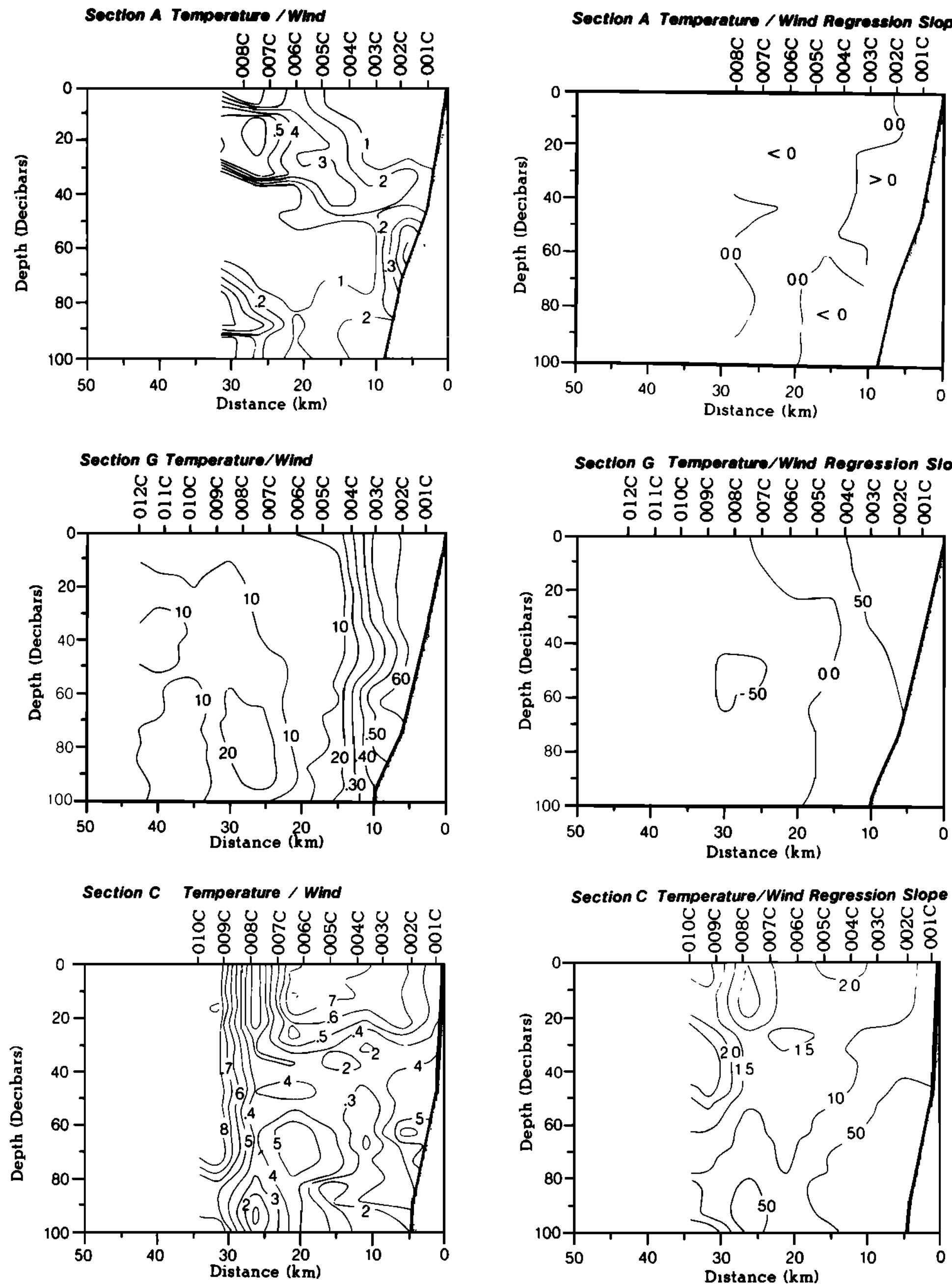

Fig. 17. Correlation coefficient and slope (°C m^{-1} s^{-1}) of the linear regression of temperature versus the wind velocity 24 hours previous at the Point Sal buoy.

the first temperature modes at the P1, P2, and P3 moorings (representing 96, 86, and 81% of the variance per mooring, respectively) lagged the winds by 1, 2, and 7 days, respectively, with maximum lagged correlations of 0.66, 0.51, and 0.50, respectively. We concluded that the lag time between winds and temperatures tended to increase as the water depth or the distance from shore increased. In a separate analysis, using individual temperatures as opposed to EOF time series, we found a slight (up to 1-day difference) tendency for wind-temperature lags at the same mooring to increase with increasing depth in the water column. On the basis of these analyses, we chose 1 day as a representative lag between winds and temperatures, and we used that in our regression analysis. The A, G, and C lines were repeated many times, forming a time series spanning a period of over 1 month. The temperatures at each space-time location were regressed against the wind from the National Data Buoy Center meteorological buoy off Point Sal (see Figure 1) 24 hours previous to the particular station time. A simple linear regression was used. The wind was rotated 45° counterclockwise to lie parallel to the Point Conception–Point Arguello shoreline.

The wind-SST and wind-subsurface temperature correlations are shown in Figures 9 and 17, respectively. The highest surface correlations (approximately 0.85) were found nearshore between the points, in a band about 20 km west of the coast north of Point Arguello, and in the middle of the channel southeast of Point Conception. Areas of surface correlation above 0.6 covered the large area that was observed to

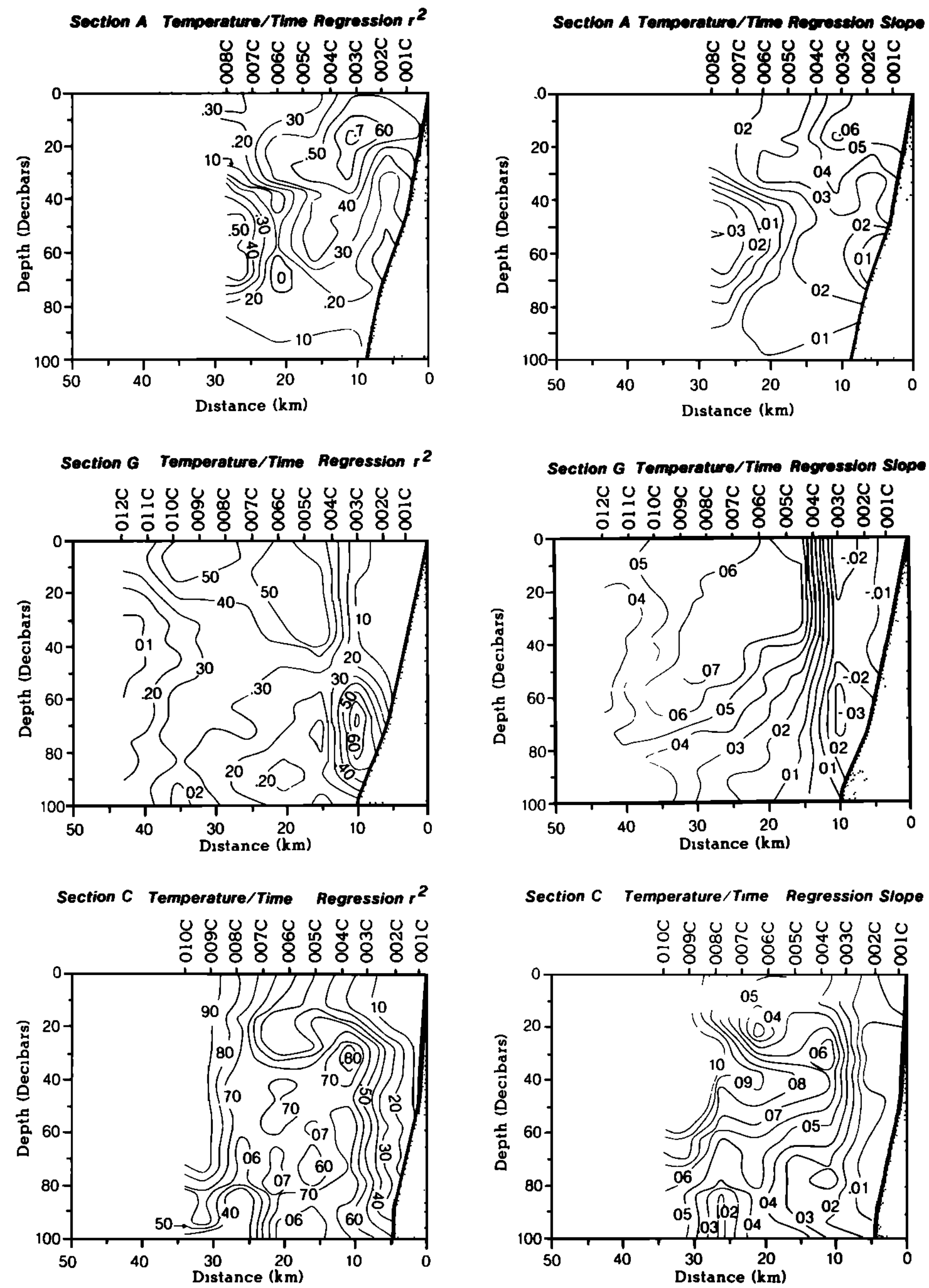

Fig. 18. Correlation coefficient and slope (°C day^{-1}) of the linear regression of temperature versus time.

be under the influence of the upwelling plumes. The depth variation of the correlations varied considerably between the three hydrographic lines. On the A line, west of Point Arguello, the high correlations were found in the offshore band at a depth of 20 m. The vertical section at the A line did not show high (>0.8) surface correlations as the SST data did, possibly because of sparse data or diurnal aliasing which was not present in the SST data. On the G line, between the points, highest correlation was nearshore as in the SST correlation. The correlation was constant with depth and decreased rapidly by 15 km offshore. The correlations were much lower than those for SST, which could be because of the different alongshore components used. On the C line, highest correlation was in the upper layer within about 20 km of the coast and then in an 80-m-deep layer about 30 km south of Point Conception. The values are similar to the SST values.

The temperature-wind correlations did not show the clear pattern,of results obtained farther north [*Huyer*, 1984], where a surface maximum was found 15 km offshore and descended as a maximum from there offshore. Our section A, which extends west from the straight coast and is similar to sections further north, might be expected to appear similar to Huyer's data, if any do, but did not.

The slope of the temperature versus wind regressions were positive, meaning that upwelling winds (negative sign) were related to colder temperatures (upwelling). The maximum magnitude of the regression slope varied from 0.5°C dyn^{-1} cm^{-2} on the G line to as high as 2.5°C dyne^{-1} cm^{-2} on the C line. This implies that the wind was more effective at causing cooling south of Point Conception than at other locations.

The temperature field was correlated against time in a separate analysis to determine if there was a simple increase of temperature with time. The resulting plots (Figure 18) indicate that the highest correlation was found on the C line with other areas of high r^2 at depth over the slope on the G line and in the upper layer about 10 km offshore on the A line. The slopes of the regressions were positive (the water was warming with time) and ranged in the areas of high correlation from 0.05°C day^{-1} to 0.10°C day^{-1}, which agrees with the approximately 0.02°–0.04°C day^{-1} increase observed at the moorings [*Brink et al.*, 1985]. The current meter records indicated that the longer-term warming observed in the shipboard records ended in early May, followed by the normal seasonal warming in late May and continuing into the summer.

7. CONCLUSIONS

We would like to restate some of the important observations and inferences from these observations. First, there appears to be no doubt, based on shipboard, aircraft, and satellite observations, that the area between points Conception and Arguello was a locus of wind-driven upwelling activity. At times, cold water appeared north of Point Arguello or east of Point Conception, but in the mean and in the synoptic observations the coldest water generally appeared between the points. There is also no doubt that the upwelling plume extended south from the points but with a great deal of directional variability within that general heading. Interestingly, and unexplained, the plume direction varied despite similar wind conditions. We suggest that the plume direction may be influenced by channel outflow or by offshore cyclonic and anticyclonic eddies. Although the upwelling events were dramatic, the effect of relaxation or downwelling favorable winds was equally impressive. With cessation of upwelling winds, a layer of fresher, warmer water invaded the area, forming a uniformly warm surface temperature field and depressed isotherms. In addition to upwelling-related distributions and circulations, longer-term warming was identified in the current meter records, and a large-scale cyclonic circulation in the channel persisted during the observational period. These phenomena may have affected the plume structure or the response of the system to wind events.

Deeper, saltier water was upwelled, creating a low-temperature, high-salinity plume. The high salinity in the upwelling plume was in contrast to the relatively low-salinity surface waters in the immediate area and even lower salinity surface waters to the west that apparently invaded the area during relaxation or downwelling.

In a very qualitative sense, the system structure looked like a typical upwelling system with properties ascending toward the coast with slight deviations possibly related to an undercurrent. However, the variability was not similar to that in northern California [*Huyer*, 1984], suggesting that the complexity of the topography was important in the variability but not in the mean. The variability near shore, within the area expected to be affected by wind-forced coastal upwelling, was related to the wind, but offshore the influence of other waters was apparent even though they were probably at least partly advected by the same wind-driven currents.

In conclusion we can say that the Point Conception–Point Arguello area is an upwelling center that rather predictably, except for plume direction, responded to the wind field. It is probable that the complex topography induced additional variability into the system than would otherwise be expected.

Acknowledgments. This work was supported by the National Science Foundation through grants OCE-8511526 to L.P.A., OCE-8506468 to K.H.B., OCE-8213872 to D.W.S., OCE-8507438 to B.H.J., and OCE-8213456 to R.E.D. The authors would like to thank the many technicians and students that assisted with the data acquisition and analysis. The color enhancements were provided by Curt Davis and Phil Zion at the Jet Propulsion Laboratory and by Charles McClain at Goddard Space Flight Center. We appreciate the professional support provided by the Research Aviation Facility of NCAR.

REFERENCES

Breaker, L., and R. P. Gilliland, A satellite sequence on upwelling along the California coast, in *Coastal Upwelling, Coastal and Estuarine Sci.*, vol. 1, edited by F. A. Richards, pp. 87–94, AGU, Washington, D. C., 1981.

Breaker, L., and C. N. K. Mooers., Oceanic variability off the central California coast, *Prog. Oceanogr.*, in press, 1986.

Brink, K. H. and R. D. Muench, Circulation in the Point Conception–Santa Barbara Channel region, *J. Geophys. Res.*, *91*, 877–895, 1986.

Brink, K. H., D. Halpern, and R. L. Smith, Circulation in the Peruvian upwelling system near 15°S, *J. Geophys. Res.*, *85*, 4036–4048, 1980.

Brink, K. H., D. W. Stuart, and J. C. Van Leer, Observation of the coastal upwelling region near 34°30′N off California: Spring 1981, *J. Phys. Oceanogr.*, *14*, 378–391, 1984.

Brink, K. H., D. Chausse, and R. E. Davis, Moored current meter and wind recorder measurements near Point Conception, California: The 1983 OPUS observations, *Tech. Rep. WHOI-85-1*, 35 pp., Woods Hole Oceanogr. Inst., Woods Hole, Mass., 1985.

Caldwell, P. C., D. W. Stuart and K. H. Brink, Mesoscale wind variability near Point Conception, California during Spring 1983, *J. Clim. Appl. Meteorol.*, *25*, 1241–1254, 1986.

Davis, R. E., Drifter observations of coastal surface currents during CODE: The method and descriptive view, *J. Geophys. Res.*, *90*, 4741–4755, 1985.

Davis, R. E., and L. Regier, Current-following drifters in OPUS-83, *SIO Ref. 84-12*, 41 pp., Scripps Inst. of Oceanogr., La Jolla, Calif., 1984.

Davis, R. E., J. E. Dufour, G. J. Parks, and M. R. Perkins, Two inexpensive current-following drifters, *SIO Ref. 82-28*, 54 pp., Scripps Inst. of Oceanogr., La Jolla, Calif., 1982.

Emery, K. O., *The Sea off Southern California*, 366 pp., John Wiley, New York, 1960.

Enfield, D. B., and J. S. Allen, On the structure and dynamics of monthly sea level anomalies along the Pacific coast of North and South America, *J. Phys. Oceanogr.*, *10*, 557–578, 1980.

Helland-Hansen, B., The Sognefjord section—Oceanographic observations in the northernmost part of the North Sea and the southern part of the Norwegian Sea, James Johnstone Memorial Volume, Lancashire Sea Fish. Lab., Liverpool, England, 1934.

Hickey, B. M., The California current system–Hypotheses and facts, *Prog. Oceanogr.*, *18*, 191–279, 1979.

Huyer, A., Hydrographic observations along the CODE Central line off northern California, 1981, *J. Phys. Oceanogr.*, *14*, 1647–1658, 1984.

Jones, B. H., K. H. Brink, R. C. Dugdale, D. W. Stuart, J. C. Van Leer, D. Blasco, and J. C. Kelley, Observations of a persistent upwelling center off Point Conception, California, *Coastal Upwelling*, part A, edited by E. Suess and J. Thiede, pp. 37–60, Plenum, New York, 1983.

Kelly, K. A., Swirls and plumes or applications of statistical methods to satellite derived surface temperatures, technical report, *Ref. 83-15*, 210 pp., Scripps Inst. of Oceanogr., La Jolla, Calif., 1983.

McClain, E. P., W. G. Pichel, C. C. Walton, C. Ahmad, and J. Sutton, Multi-channel improvements to satellite-derived global sea surface temperatures, *Adv. Space Res.*, *2*, 43–47, 1983.

Mooers, C. N. K., and A. R. Robinson, Turbulent jets and eddies in the California Current and inferred cross-shore transports, *Science*, *223*, 51–53, 1984.

Reid, J. L., Jr., Physical oceanography of the region near Point Arguello, technical report, *IMR Ref. 75-19*, 30 pp., Inst. of Mar. Res., Univ. of Calif., La Jolla, 1965.

Reid, J. L., Jr., and A. W. Mantyla, The effect of the geostrophic flow upon coastal sea elevations in the northern North Pacific Ocean, *J. Geophys. Res.*, *81*, 3100–3119, 1976.

Rienecker, M. M., C. N. K. Mooers, D. E. Hagan, and A. R. Robinson, A cool anomaly off northern California: An investigation using IR imagery and in situ data, *J. Geophys. Res.*, *90*, 4807–4818, 1985.

Sverdrup, H. V., On the process of upwelling, *J. Mar. Res.*, *2*, 155–164, 1938.

Traganza, E. D., D. A. Nestor, and A. K. McDonald, Satellite observations of nutrient upwelling off the coast of California, *J. Geophys. Res.*, *85*, 4101–4106, 1980.

L. P. Atkinson, Department of Oceanography, Old Dominion University, Norfolk, VA 23508.

K. H. Brink, Woods Hole Oceanographic Institution, Woods Hole, MA 02543.

R. E. Davis, Scripps Institution of Oceanography, La Jolla, CA 92093.

B. H. Jones, Department of Biological Sciences, University of Southern California, Los Angeles, CA 90089.

T. Paluszkiewicz, School of Oceanography, Oregon State University, Corvallis, OR 97331.

D. W. Stuart, Department of Meteorology, Florida State University, Tallahassee, FL 32306.

(Received April 3, 1986;
accepted May 27, 1986.)

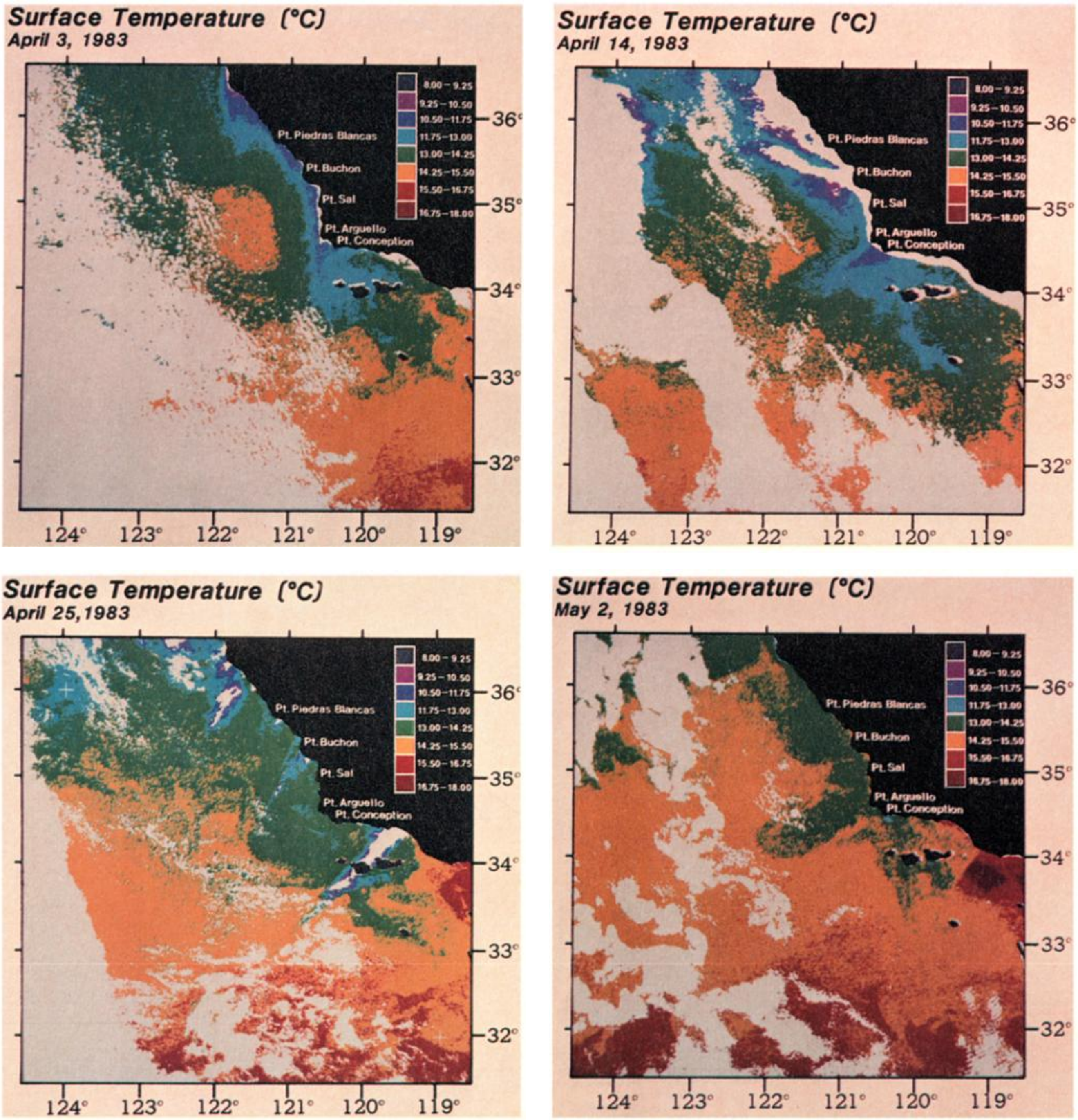

Plate 1 [*Atkinson et al.*]. Surface temperature from the NOAA 7 AVHRR. The mean and variance of the temperatures are also shown. The data are valid around the Point Arguello–Point Conception area and are less valid elsewhere because of clouds. Thus the reader should focus mainly on the upwelling plume extending from the points and less on offshore structures and features along the coast north of Point Arguello unless it is specifically mentioned in the text. The statistics in the vicinity of the plume are valid, but those along the north coast and in the western and southwest portion of the images are inaccurate.

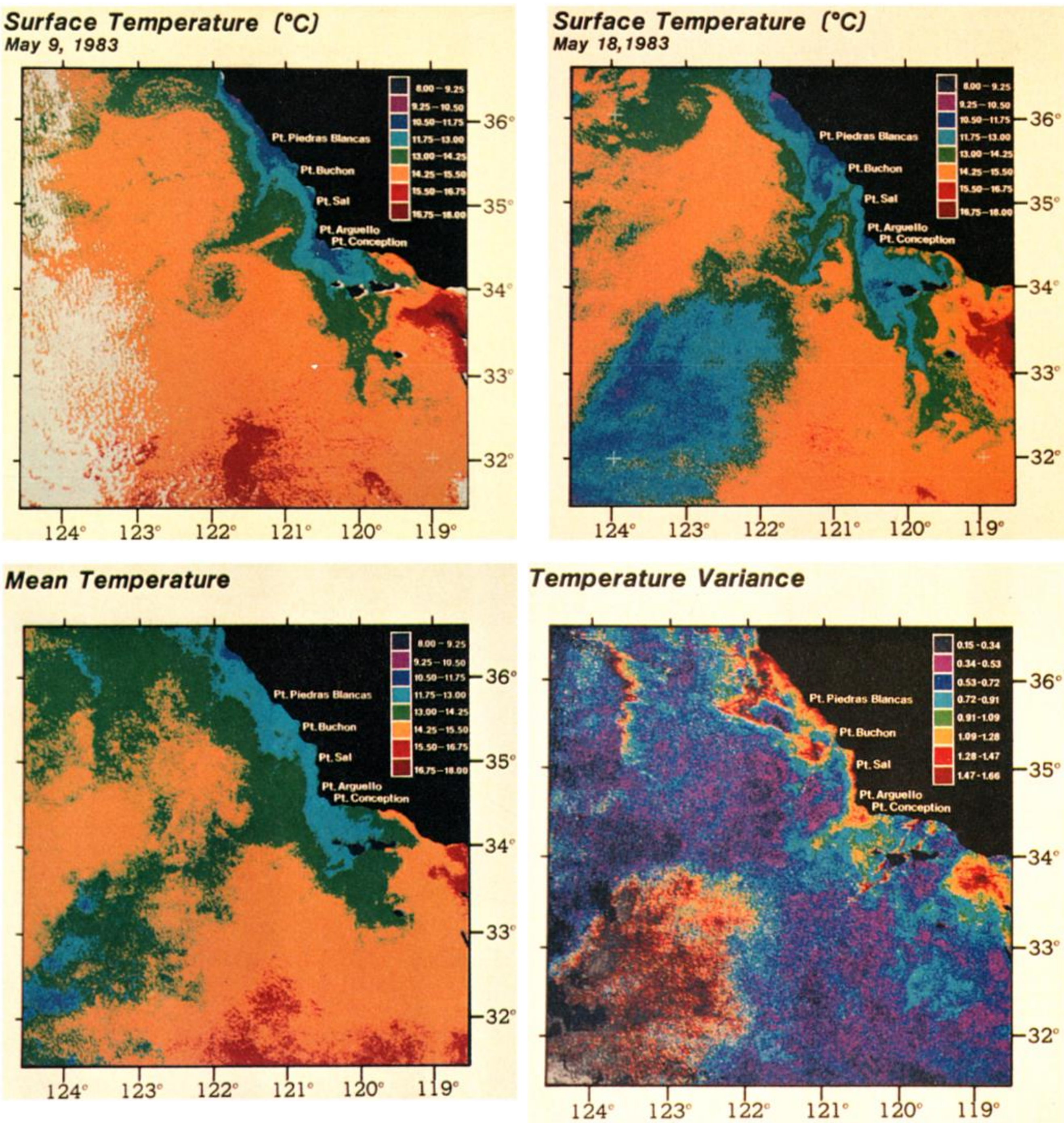

Plate 1 [*Atkinson et al.*]. (continued)